

RESEARCH

Open Access



# Gut bacterium *Intestinimonas butyriciproducens* improves host metabolic health: evidence from cohort and animal intervention studies

Elena Rampanelli<sup>1,2†</sup>, Nadia Romp<sup>1,2†</sup>, Antonio Dario Troise<sup>3</sup>, Jakshana Ananthasabesan<sup>1</sup>, Hao Wu<sup>4</sup>, Ismail Sahin Gül<sup>5</sup>, Sabrina De Pascale<sup>3</sup>, Andrea Scaloni<sup>3</sup>, Fredrik Bäckhed<sup>6</sup>, Vincenzo Fogliano<sup>7</sup>, Max Nieuwdorp<sup>1</sup> and Thi Phuong Nam Bui<sup>1,8\*</sup>

## Abstract

**Background** The human gut microbiome strongly influences host metabolism by fermenting dietary components into metabolites that signal to the host. Our previous work has shown that *Intestinimonas butyriciproducens* is a prevalent commensal bacterium with the unique ability to convert dietary fructoselysine to butyrate, a well-known signaling molecule with proven health benefits. Dietary fructoselysine is an abundant Amadori product formed in foods during thermal treatment and is part of foods rich in dietary advanced glycation end products which have been associated with cardiometabolic disease. It is therefore of interest to investigate the causal role of this bacterium and fructoselysine metabolism in metabolic disorders.

**Results** We assessed associations of *I. butyriciproducens* with metabolic risk biomarkers at both strain and functional levels using a human cohort characterized by fecal metagenomic analysis. We observed that the level of the bacterial strain as well as fructoselysine fermentation genes were negatively associated with BMI, triglycerides, HbA1c, and fasting insulin levels. We also investigated the fructoselysine degradation capacity within the *Intestinimonas* genus using a culture-dependent approach and found that *I. butyriciproducens* is a key player in the butyrogenic fructoselysine metabolism in the gut. To investigate the function of *I. butyriciproducens* in host metabolism, we used the diet-induced obesity mouse model to mimic the human metabolic syndrome. Oral supplementation with *I. butyriciproducens* counteracted body weight gain, hyperglycemia, and adiposity. In addition, within the inguinal white adipose tissue, bacterial administration reduced inflammation and promoted pathways involved in browning and insulin signaling. The observed effects may be partly attributable to the formation of the short-chain fatty acids butyrate from dietary fructoselysine, as butyrate plasma and cecal levels were significantly increased by the bacterial strain, thereby contributing to the systemic effects of the bacterial treatment.

**Conclusions** *I. butyriciproducens* ameliorates host metabolism in the context of obesity and may therefore be a good candidate for new microbiota-therapeutic approaches to prevent or treat metabolic diseases.

<sup>†</sup>Elena Rampanelli and Nadia Romp equally contributed to this work and are designated as co-first authors.

\*Correspondence:

Thi Phuong Nam Bui  
t.p.n.bui@amsterdamc.nl

Full list of author information is available at the end of the article



## Introduction

Diet, the human microbiome, and host genetics are determinants of metabolic status, in part through the production of metabolites via fermentation of dietary components by the gut microbiota [1, 2]. Understanding the metabolism of dietary components by the microbiome is key to mediating the effects of the human microbiome on host metabolism. Mechanistic studies of the interactions between dietary components, the microbiome, and the host are therefore urgently needed. Of great interest is the ability of the gut microbiota to metabolize dietary compounds that are abundantly produced during food processing: are they harmful xenobiotics or is the human microbiota capable of metabolizing them for good?

Fructoselysine is an abundant Amadori product formed by the non-enzymatic reaction between a reducing sugar and amino acids in foods during thermal processing and storage. The formation of Amadori compounds partially blocks amino acids from absorption, thereby reducing their bioavailability to the host [3]. It is estimated that the daily intake of Amadori products is approximately 0.5–1 g, of which the vast majority reaches the colon for further digestion in healthy individuals [4]. More importantly, due to the reaction kinetics and the availability of free amino groups, there is simultaneous formation and oxidative fragmentation of Amadori compounds to form  $\alpha$ -dicarbonyls and subsequently advanced glycation end products (AGEs), such as CML and CEL [5]. These dietary AGEs have been associated with cardiovascular risks and diabetic complications [6–8]. To date, few intestinal bacteria have been reported to metabolize fructoselysine. Some probiotic strains, mainly *Bifidobacterium* and *Lactobacillus* spp. have been reported to convert fructoselysine to glucose and lysine and subsequently utilize the liberated glucose moiety but not lysine [9]. *E. coli* is able to degrade fructoselysine and use the released glucose for growth in vitro [10], while *Collinsella intestinalis* can metabolize fructoselysine to acetate and formate both in vitro and in vivo [11]. All these strains failed to use the liberated lysine moiety for growth. *Intestinimonas butyriciproducens* showed exceptional metabolic properties being able to use both the glucose and lysine moiety released from fructoselysine degradation to form butyrate via two separate pathways [12]. The conversion of fructoselysine to butyrate is highly desirable. Butyrate serves as an energy source for colonocytes but also suppresses inflammation in various tissues [13–15] and is involved in the regulation of insulin release via gut hormone stimulation [14, 16]. This is in line with numerous reports on the depletion of butyrate-producing species in diabetic and obese subjects and supplementation of these species provided the metabolic benefits to the

host [17–19]. It is therefore of great interest to explore the therapeutic potential of *I. butyriciproducens* in improving metabolic health via its unique ability to convert fructoselysine to butyrate.

In this study, we investigated the associations between butyrogenic *Intestinimonas butyriciproducens* and fructoselysine pathway genes and metabolic risk biomarkers in metabolically compromising individuals compared to healthy controls in the Swedish Impaired Glucose Tolerance (IGT) cohort ( $n=1011$ ) [20]. We then isolated 4 human *Intestinimonas* isolates and studied their fructoselysine fermentation capacity and genomic characteristics. We later administered the *Intestinimonas butyriciproducens* GL3 isolate to diet-induced obese mice to investigate the effects on obesity and host metabolism and to gain mechanistic understanding that is important for future proof-of-concept studies in humans.

## Results

### *Intestinimonas butyriciproducens* and fructoselysine fermentation were reduced in subjects with high metabolic risks

To investigate whether *Intestinimonas butyriciproducens* is associated with host metabolic health, we used metagenomic data from a Swedish cohort of 1011 individuals with pre-diabetes and treatment-naïve type 2 diabetes (T2D) and healthy relatives [20]. Comparing the rarefied read abundances of *I. butyriciproducens* in subjects with different glycemic statuses ranging from normal glucose tolerance to T2D, we observed that the relative abundance of *I. butyriciproducens* was significantly reduced in groups with impaired fasting glucose (IFG,  $P=0.034$ ), impaired glucose tolerance (IGT,  $P=0.02$ ), combined glucose intolerance (CGI,  $P=0.021$ ) and type 2 diabetes (T2D,  $P=0.055$ ) as compared to low-risk normal glucose tolerance (lrNGT) but not to high-risk normal glucose tolerance (hrNGT) (Fig. 1A). To further explore associations of *I. butyriciproducens* with metabolic risk factors, we correlated the relative abundance of identified fructoselysine pathway genes and bacterial levels [12] with metabolic biomarkers (Fig. 1B). This previously identified pathway consists of four main functions: fructoselysine uptake and degradation, lysine utilization, butyrate formation from glucose-6-phosphate and butyrate formation from lysine (Fig. 1B, Supplementary Table S1). We found that both the abundance of these functional group genes (either individually or as a group) and *Intestinimonas butyriciproducens* levels were negatively associated with metabolic risk, including triglycerides, BMI, fasting glucose, and 2 h OGTT glucose. Genes involved in lysine utilization and the formation of butyrate from lysine were found to have stronger associations

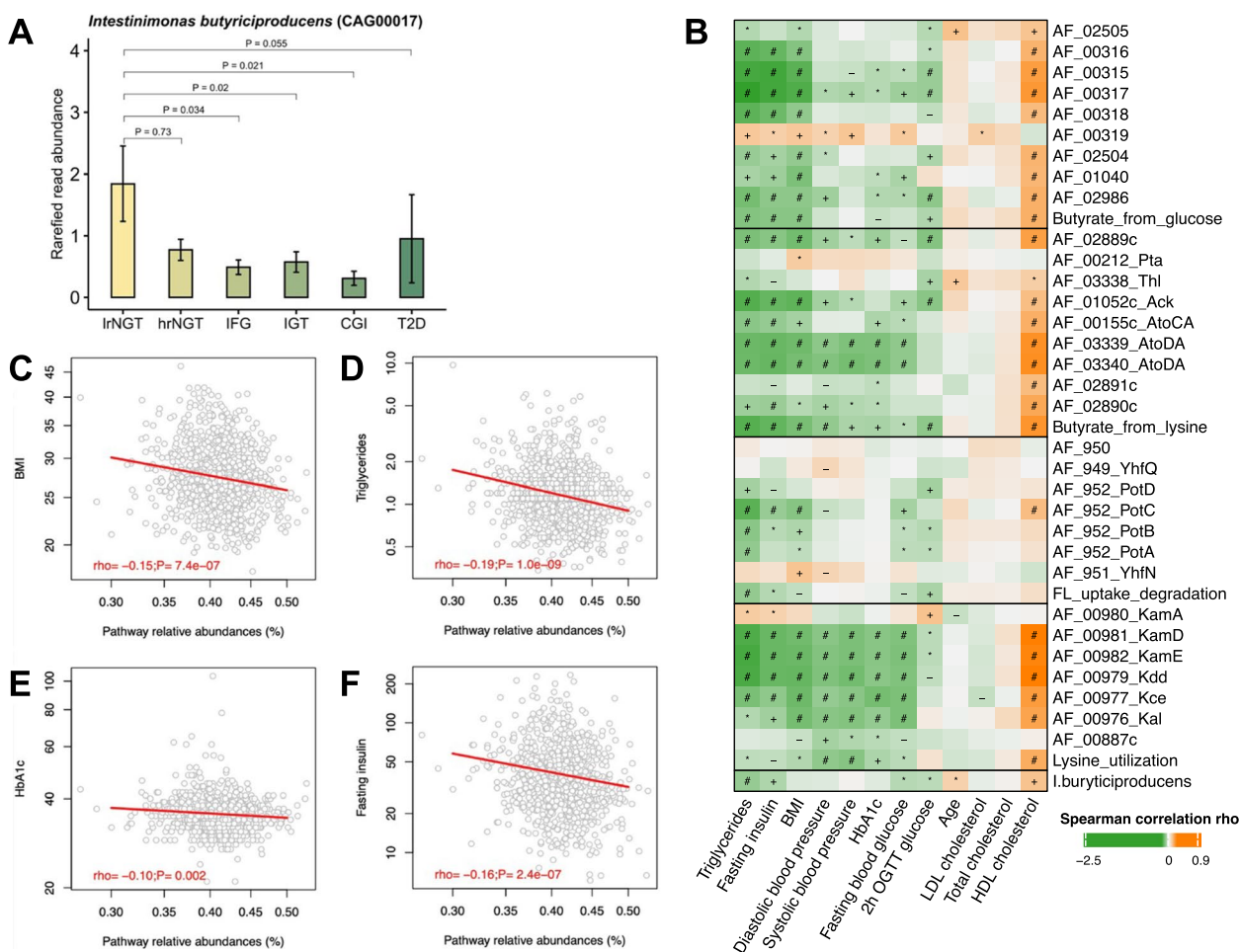


**Fig. 1** Negative associations between *Intestinimonas butyriciproducens* and fructoselysine fermentation genes and metabolic biomarkers in the human cohort. **A** Significant reduction of *Intestinimonas butyriciproducens* in IFG (impaired fasting glucose), IGT (impaired glucose tolerance), CGI (combined glucose intolerance), hrNGT (high-risk normal glucose tolerance) and T2D groups as compared to IrNGT (low-risk normal glucose tolerance) control based on rarefied reads of *Intestinimonas butyriciproducens* in a Swedish prediabetes cohort ( $n = 1011$ ; Spearman correlation). **B** Metagenomic analysis shows negative associations of individual FL pathway genes with different metabolic biomarkers (Wilcoxon rank-sum test).  $-P < 0.1$ ;  $*P < 0.05$ ;  $+P < 0.01$ ;  $\#P < 0.001$ . The fructoselysine (FL) degradation pathway consists of 4 separate sub-pathways: FL uptake and degradation, lysine utilization, butyrate from lysine, and butyrate from glucose-6-phosphate. The correlations of these individual sub-pathways with each metabolic biomarker are shown. **C–F** Significant negative associations between FL pathway gene abundance and BMI (body mass index,  $P = 7.4e-07$ ) (**C**), triglycerides ( $P = 1.0e-09$ ) (**D**), HbA1c (hemoglobin A1c,  $P = 0.002$ ) (**E**) and fasting insulin ( $P = 2.4e-07$ ) (**F**), respectively

than those involved in fructoselysine degradation and butyrate formation from glucose-6-phosphate, suggesting that the conversion of lysine to butyrate may be beneficial for metabolic health. Notably, two genes involved in fructoselysine degradation: fructoselysine kinase (AF\_949) and fructosamine deglycase (AF\_00951) were not associated with risk factors, which may be explained by the presence of these two genes in the genomes of some pathogenic strains, including *E. coli* and *Salmonella*, which are commonly found in the human feces [10, 21]. However, these bacteria are

unable to ferment lysine or produce butyrate. Thus, the association of these two fructoselysine conversion genes did not represent the ability of the microbiome to convert fructoselysine to butyrate. To investigate the associations of *Intestinimonas butyriciproducens* with metabolic risks via its unique ability to convert fructoselysine to butyrate, we examined the associations between the total abundance of fructoselysine pathway genes and metabolic markers. We found significant negative correlations between the relative abundance of the fructoselysine pathway and body mass index (BMI,  $\rho = -0.15$ ;  $P = 7.4e-07$ ), triglycerides ( $\rho = -0.19$ ;  $P = 1.0e-09$ ), glycated haemoglobin (HbA1c,  $\rho =$

-0.10;  $P=0.002$ ), and fasting insulin ( $\rho = -0.16$ ;  $P=2.4e-07$ ) (Fig. 1C–F), suggesting a reduced capacity to convert fructoselysine to butyrate in the microbiome of subjects at high metabolic risk. These results are consistent with the observed reduced abundance of *I. butyriciproducens* in individuals with T2D or impaired glucose tolerance.

***Intestinimonas* as a key player in the butyrogenic fructoselysine metabolism in the gut**

To investigate the ability of *Intestinimonas* to ferment fructoselysine, we next performed a conventional cultivation technique using a selective medium on an agar plate to isolate *Intestinimonas* species from the human stools of three healthy volunteers. We obtained three *Intestinimonas* isolates and subsequently sequenced the 16S rRNA genes and genomes to allow further genomic and physiological characterization. To determine the taxonomic relationship of these isolates, a phylogenetic tree was constructed using 16S rRNA gene sequences from three *Intestinimonas* isolates (strains GL3, IY4, and AS-BT) and other closely related species in *Clostridium* cluster IV (in green) and cluster XIVa (in orange) (Fig. 2A). While the 16S rRNA genes of the two strains IY4 and GL3 were highly similar (>99.7 %) to *Intestinimonas butyriciproducens* type strain DSM26588<sup>T</sup> (isolated from mouse cecum) [22] and previously isolated *Intestinimonas* strain AF211, the 16S rRNA gene of the strain AS-BT was only 95 % similar to that of the type of strain, suggesting the strain AS-BT probably represents

a new species of the *Intestinimonas* genus. Nevertheless, all three *Intestinimonas* isolates were able to grow and convert fructoselysine and lysine to butyrate and acetate with a similar degradation rate (Fig. 2B–E) and have complete fructoselysine pathway genes in their genomes (Supplementary Table S2). Interestingly, we found that strain AS-BT did not have a complete vitamin B12 pathway in its genome, whereas three other strains did (Supplementary Table S3), indicating the potential ability of strain GL3 and IY4 to synthesize pseudovitamin B12 as strain AF211 [23].

Antibiotic resistance at both functional and genomic levels is relevant to gut bacteria as it may imply the potential transfer of the antibiotic resistance capacity via horizontal gene transfer to the gut microbiome of recipients [24], and this is of particular interest for new generation therapeutic strains. We determined the minimum inhibitory concentration (MIC) of different antibiotics as well as antibiotic resistance genes in their bacterial genomes in four strains using Etest (Supplementary Table S4). AS-BT clearly had a distinctly different MIC profile as compared to the other three strains (GL3, IY4, and AF211) which may be attributed to the distant taxonomic position of this strain from three other *Intestinimonas* isolates. In general, *Intestinimonas* isolates were susceptible to teicoplanin, chloramphenicol, vancomycin, cefotaxime, and oxacillin, which are inhibitors of cell wall synthesis in Gram-positive bacteria, but they showed relatively high MIC values with ciprofloxacin and sulfamethoxazole, but no gene was attributed to resistance

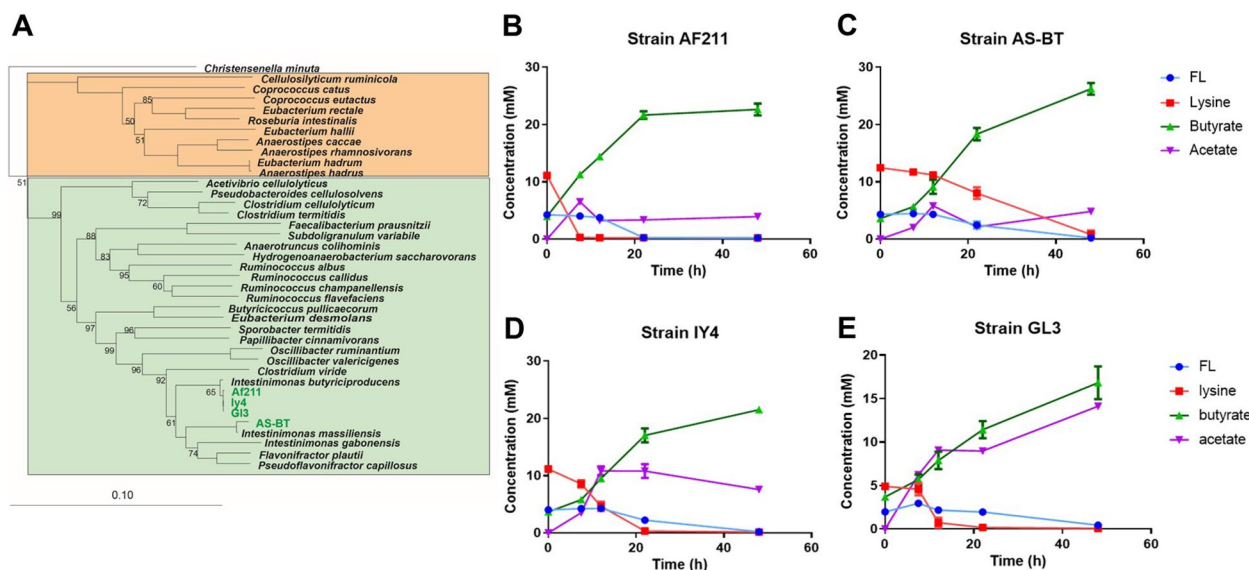


**Fig. 2** *Intestinimonas* isolates and fructoselysine conversion. **A** A phylogenetic tree based on 16S rRNA genes from 4 *Intestinimonas* human isolates and *Intestinimonas butyriciproducens* DSM26588<sup>T</sup> (the type strain) and closely related species. Orange: species in *Clostridium* cluster XIVa and green: species in *Clostridium* cluster IV. Bar represents 10 % sequence divergence (**B–E**) fructoselysine conversion by *Intestinimonas* strain GL3, IY4, AS-BT and AF211. All data are presented as mean values ± SD ( $n=2$  biological replicates). FL: fructoselysine

mechanisms for these two antibiotics. Although some vancomycin resistance genes (*vanB*, *vanW*, *vanS*, and *vanR*) were detected in the genomes (Supplementary Table S5), these genes were not sufficient to form a complete operon conferring vancomycin resistance [25]. Two out of the four strains were resistant to erythromycin at very high levels, while all four strains were resistant to tetracycline at varying levels (from 2 to 16 µg/ml). Notably, the tetracycline resistance gene *tetW* was not found in the genome of GL3 whereas *tetW* was present in all the genomes from three other *Intestinimonas* strains. In contrast, a large number of gene copies for efflux pumps were found in all *Intestinimonas* genomes, with the highest number of 27 pumps from GL3 isolate, which may be an important mechanism to eliminate toxic compounds.

#### ***Intestinimonas butyriciproducens* limits body weight gain in mice fed a high-fat diet**

Butyrate is known to be a signaling molecule that can modulate glucose metabolism and insulin sensitivity [26]. A decrease in both intestinal butyrate production and butyrate-producing bacteria in T2D has been observed in multiple cohorts [27, 28]. This is consistent with our observations in the Swedish (pre)diabetes cohort. Therefore, supplementation with butyrate-producing bacteria may have therapeutic effects in the prevention or treatment of type 2 diabetes. As strain GL3 has a favorable antibiotic resistance profile with the absence of *tetW*, we use *Intestinimonas butyriciproducens* GL3 strain (hereafter referred to as IB) to investigate the effects of *Intestinimonas butyriciproducens* on systemic host metabolism, using the mouse diet-induced obesity (DIO) model [29]. C57BL/6 J mice were fed a high-fat diet (HFD) or a matched low-fat diet (LFD) for 13 weeks and subjected to oral gavage 3 times a week of placebo (only anaerobic PBS without bacteria) or IB solution. Importantly, the HFD contains significantly higher levels of protein-bound fructoselysine as compared to a regular chow diet (Supplementary Figure S1; 128.3 versus 567.5 mg/100 g protein,  $p < 0.0001$ ), making HFD an excellent source of dietary fructoselysine for butyrate production by IB. The high levels of FL in the HFD are probably due to the thermal processing with the high sugar and protein content.

Although we did not observe changes in food intake between placebo and IB-treated mice, bacterial administration resulted in significantly less body weight gain in the HFD-fed mice as compared to placebo treatment (Fig. 3A; 15.1 g versus 11.5 g,  $p = 0.038$ ). The difference in body weight between the placebo and IB groups became apparent after 11 weeks suggesting that the bacterium only affects the host only after a prolonged treatment and/or that the bacterial treatment becomes effective when mice develop exacerbated adiposity/metabolic

dysregulation. Notably, the bacterial supplementation had no effects on body weight in the LFD-fed mice.

As butyrate-producing bacteria have been associated with insulin sensitivity in both human and mouse studies [26], we next assessed blood glucose levels in the fasting state and following intraperitoneal insulin injection. As expected, HFD feeding increased the fasting glucose levels and bacterial supplementation significantly lowered fasting glucose concentrations (Fig. 3B; 11.3 mM versus 9.4 mM glucose,  $p = 0.035$ ). During the insulin tolerance test, blood glucose levels in IB-treated mice were consistently lower than in placebo mice, with significantly lower levels at 45 min after glucose administration (7.3 versus 5.6 mM glucose,  $p = 0.0416$ ), suggesting an improvement of insulin sensitivity (Fig. 3C). Analysis of the area under the curve (AUC) showed a trend towards a reduced glucose rate over time (Fig. 3D; AUC of 48.41 versus 42.08,  $p = 0.057$ ) following bacterial administration.

#### ***Intestinimonas butyriciproducens* counteracts the fat accumulation and promotes lipid degradation and browning processes in inguinal white adipose tissue**

Analysis of white adipose tissue (WAT) revealed a reduction in subcutaneous/inguinal white adipose tissue (iWAT) in IB-treated mice on HFD (2.43 versus 1.58 % BW,  $P = 0.023$ ), while the proportion of visceral/epididymal white adipose tissue (eWAT) relative to total body weight was unchanged between placebo and IB groups (Fig. 3E, F).

Since IB intake led to a reduction in the proportion of iWAT tissue, we next examined the expression of key metabolic genes in iWAT. We found that the expression of genes involved in mitochondrial metabolism and, in particular fatty acid oxidation, was strongly up-regulated following IB treatment in HFD-fed mice. Indeed, IB supplementation reduced the HFD-induced expression of *Ppargc1a4* (peroxisome proliferator-activated receptor gamma coactivator 1-alpha, 0.007108 versus 0.01577,  $P = 0.037$ ), *Ppara* (peroxisome proliferator-activated receptor alpha, 0.009667 versus 0.03057,  $P = 0.025$ ), and *Cpt1a* (carnitine palmitoyltransferase 1A, 0.1497 versus 0.3879,  $P = 0.017$ ) to levels similar to those observed in LFD-treated mice (Fig. 4A–C). In contrast, the expression rates of the browning markers were downregulated in the HFD feeding but upregulated by oral IB treatment (Fig. 4D–H). Indeed, compared to placebo, bacterial supplementation in obese mice resulted in a significantly increased expression of the browning markers *Ucp1* (uncoupling protein 1, 0.009592 versus 0.01908,  $P = 0.043$ ), *Cidea* (cell death-inducing DFFA Like Effector A, 0.08147 versus 0.2776,  $P = 0.023$ ), *Prdm16* (PR domain containing 16,

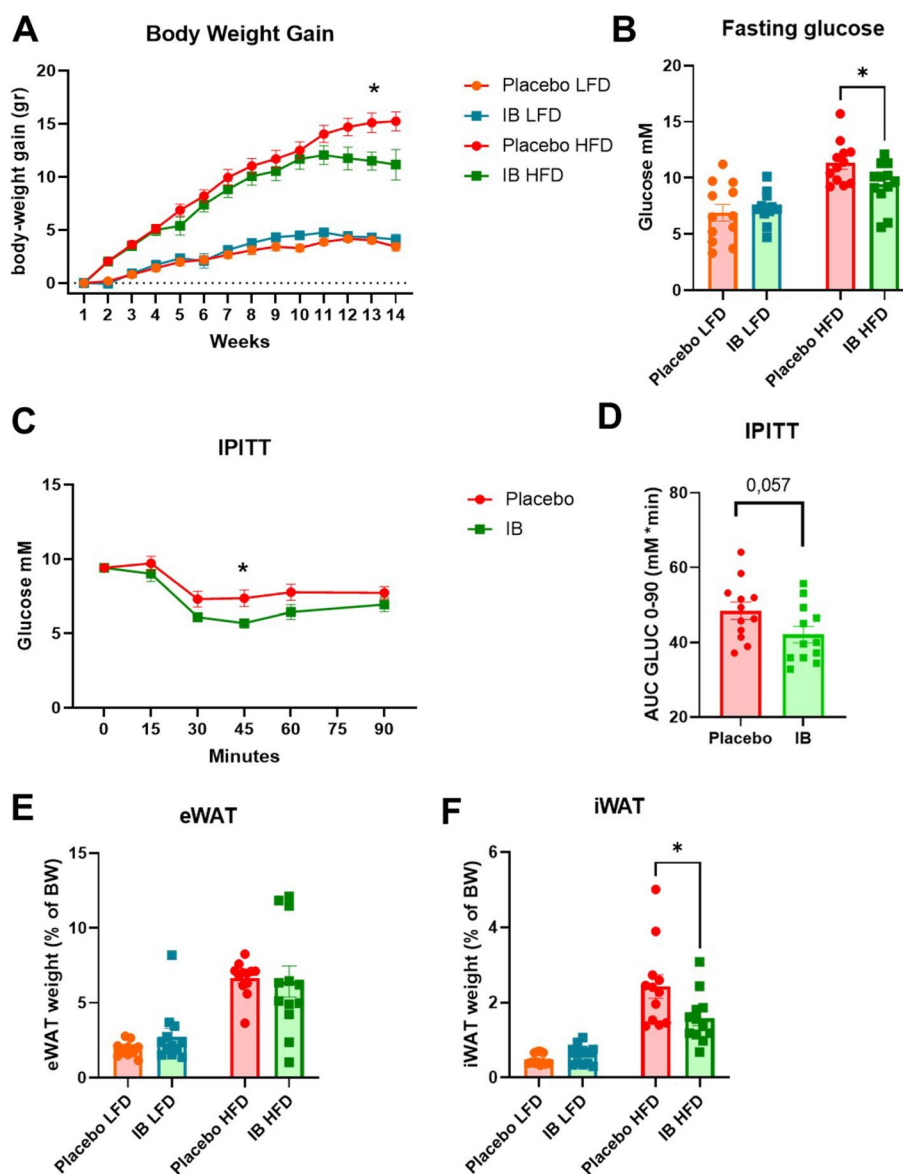


**Fig. 3** Diet-induced obesity mouse model: systemic effects of *Intestinimonas butyriciproducens* GL3 (IB). **A** Body weight gain, shown as the difference in body weight compared to baseline. **B** Fasting blood glucose levels assessed at the end of the study. **C, D** Intraperitoneal insulin tolerance test (IPITT): blood glucose levels before and after insulin injection (**C**) and area under the curve (AUC) of glucose excursion during IPITT (mM\*minute) (**D**). **E, F** Relative weight of epididymal (eWAT) and inguinal white adipose tissue (iWAT), shown as a percentage of total body weight. Statistical differences between placebo and IB groups were assessed using the non-parametric Mann–Whitney *U* test. All data are presented as mean values ± SEM (*N* = 12/group). \**P* < 0.05

0.04065 versus 0.1585, *P* = 0.0023), *Dio2* (Iodothyronine deiodinase 1, 0.03754 versus 0.2598, *P* = 0.054) and *Tbx1* (0.04912 versus 0.1597, *P* = 0.015). Based on these observations, we next assessed protein levels of PGC1α, CPT1, UCP1, and PRDM16 and found higher, although not significant, protein levels of PRDM16, UCP1, and PGC1α (Supplementary Figure S2A–E). As the transcriptional reprogramming observed in iWAT suggests an increase in energy expenditure and thermogenesis,

we then asked whether similar changes occur in the brown adipose tissue (BAT). However, in BAT we did not find significant differences in the expression of genes involved in lipid and mitochondrial metabolism nor thermogenesis between the placebo and IB treatment groups (Supplementary Figure S3).

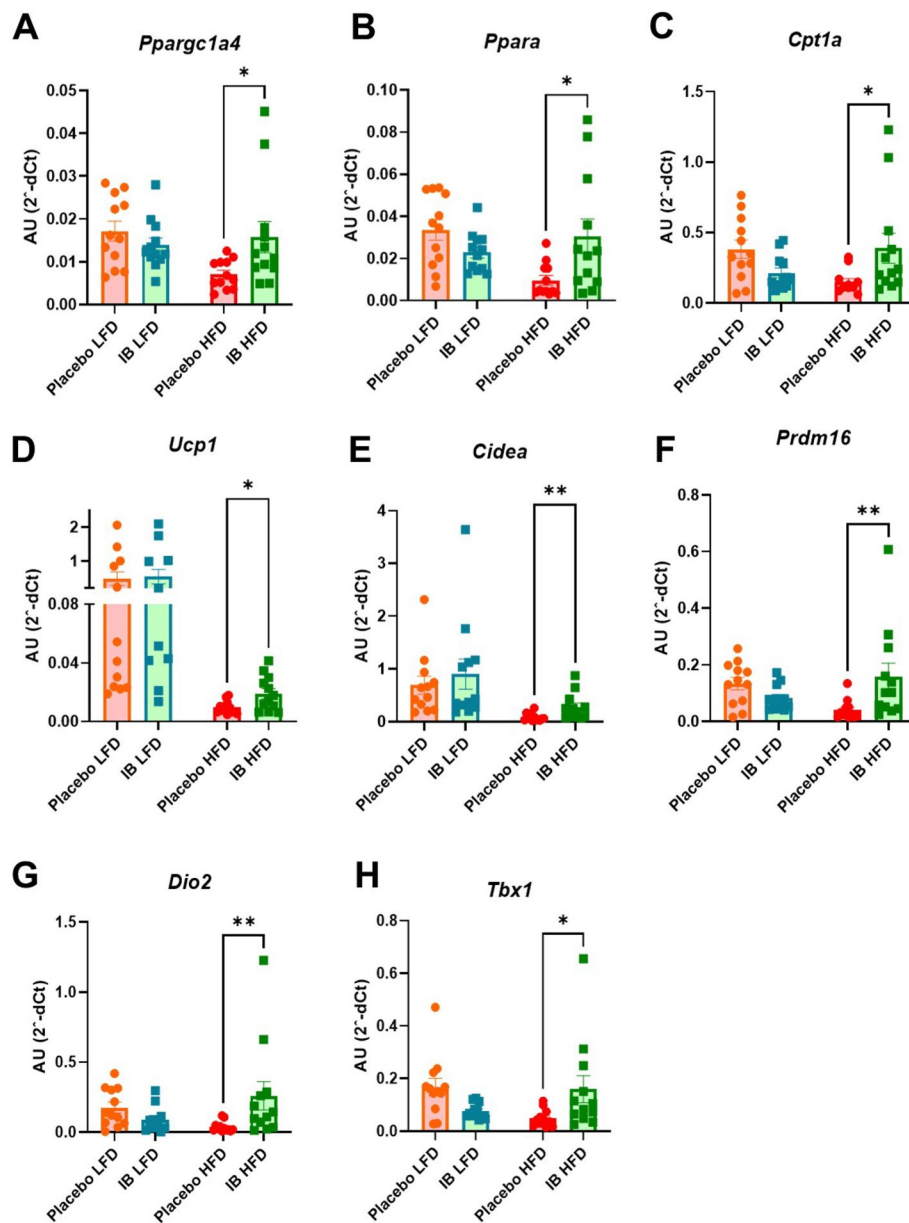


**Fig. 4** Inguinal white adipose tissue: gene expression after placebo and IB treatment. **A–H** Expression of genes encoding for proteins involved in **A–C** mitochondrial oxidative metabolism and fatty acid oxidation and in **D–H** WAT browning. Data are shown as 2<sup>-dCt</sup>. Data are presented as mean ± SEM (N = 12/group). Mann–Whitney U test was used for statistical analysis between placebo and IB groups. \*P < 0.05, \*\*P < 0.01. *Pparg1a4*: peroxisome proliferative activated receptor, gamma, coactivator 1-alpha, *Ppara*: Peroxisome proliferator-activated receptor alpha, *Cpt1a*: carnitine palmitoyl transferase 1-A, *Ucp1*: uncoupling protein 1, *Cidea*: cell death-inducing DFFA fragmentation like effector A, *Prdm16*: PR domain containing 16, *Dio2*: lodothyronine deiodinase 2, *Tbx1*: T-Box protein 1

***Intestinimonas butyriciproducens* constrains white adipose tissue inflammation and loss of insulin sensitivity in obesity**

As WAT is an important modulator of systemic insulin sensitivity [30] and IB intake augmented glucose uptake after insulin injection, we next measured the intra-iWAT expression of *Irs2* (insulin receptor substrate 2),

which mediates the cytoplasmic signaling of insulin [31]. Expression of *Irs2* was markedly diminished in iWAT of obese mice, and in line with the amelioration of insulin resistance, IB treatment resulted in increased expression of *Irs2* at both gene (Fig. 5A; 0.146 versus 0.3123, P = 0.0029) and protein levels (Fig. 5B; 0.314 versus 0.8455, P = 0.0086).

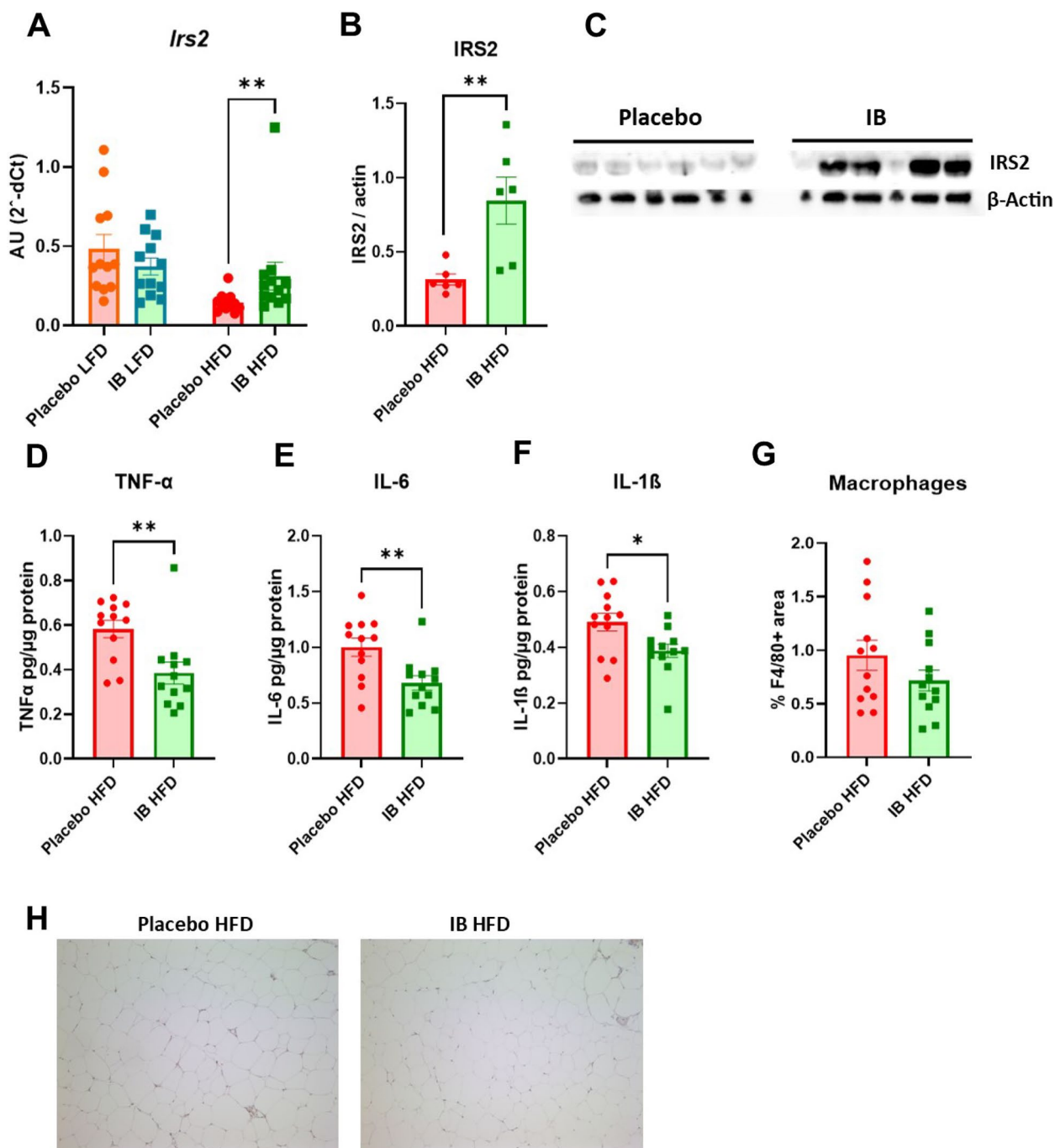


**Fig. 5** Inguinal white adipose tissue: insulin receptor and cytokine levels. **A** Expression of *Irs2* gene mRNA transcripts in inguinal WAT tissues from HFD-fed mice. **B** IRS2 protein expression levels in iWAT tissues from HFD-fed mice. IRS2 (insulin receptor substrate 2) levels are normalized to beta-actin levels. **C** Images of western blots assessing of IRS-2 and actin gene expression. **D–F** Pro-inflammatory cytokine levels detected in lysate of iWAT tissue from obese mice and normalized to protein concentrations. **G** Macrophage infiltration of iWAT, determined by immunohistochemical staining on FFPE (formalin-fixed paraffin-embedded). **(H)** Representative images were taken at  $\times 10$  magnification of F4/80 immunohistochemical staining and hematoxylin counterstaining on FFPE sections from placebo and IB-treated DIO mice section. Data are shown as a percentage of positive areas of the total area analyzed. All data are presented as mean values  $\pm$  SEM ( $N = 12$ /group). Mann–Whitney U test was used for statistical analysis.  $*P < 0.05$ ,  $**P < 0.01$ . TNF- $\alpha$ : tumor necrosis factor-alpha, IL-6: interleukin-6, IL-1 $\beta$ : interleukin-1 beta. IB: *Intestinimonas butyriciproducens* GL3 strain

As the development of insulin resistance and adipose tissue inflammation are intertwined, we subsequently examined the production of relevant pro-inflammatory cytokines by iWAT in obese mice. This revealed that intestinal IB exerted anti-inflammatory effects, as IB treatment significantly reduced the intra-WAT secretion of tumor necrosis factor (TNF)- $\alpha$  (0.5837 versus 0.3859,  $P=0.0048$ ), interleukin (IL)-6 (1.003 versus 0.6825,  $P=0.0053$ ) and IL-1 $\beta$  (0.4915 versus 0.3886,  $P=0.0165$ ) (Fig. 5D–F). In addition, staining for the macrophage marker F4/80 showed that macrophage recruitment was reduced, although not significantly, in IB-treated mice (Fig. 5G–H), possibly indicating that immune infiltrating cells as well as parenchymal cells were the source of the detected pro-inflammatory cytokines.

**Oral intake of *Intestinimonas butyriciproducens* increases levels of cecal and plasma SCFAs butyrate and acetate**

The short-chain fatty acids produced by the gut microbiome have been shown to affect metabolism in both the local gut and peripheral organs [16, 32]. Peripheral effects include the liver [33], adipose tissue [34], and the cardiovascular system [35]. To elucidate the mechanism of action of the bacterial treatment, we measured cecal and circulating levels of SCFAs. Plasma levels of butyrate and acetate were significantly increased in obese mice after IB treatment as compared to placebo (butyrate: 0.9817 versus 1.12  $\mu\text{M}$ ,  $P=0.0367$ ; acetate: 374.3 versus 664.3  $\mu\text{M}$ ,  $P=0.0068$ ) (Fig. 6A, B). Although the plasma fructoselysine concentrations were similar between the groups (Supplementary Figure S4A), the butyrate/fructoselysine ratio tended to increase in the HFD-fed mice receiving

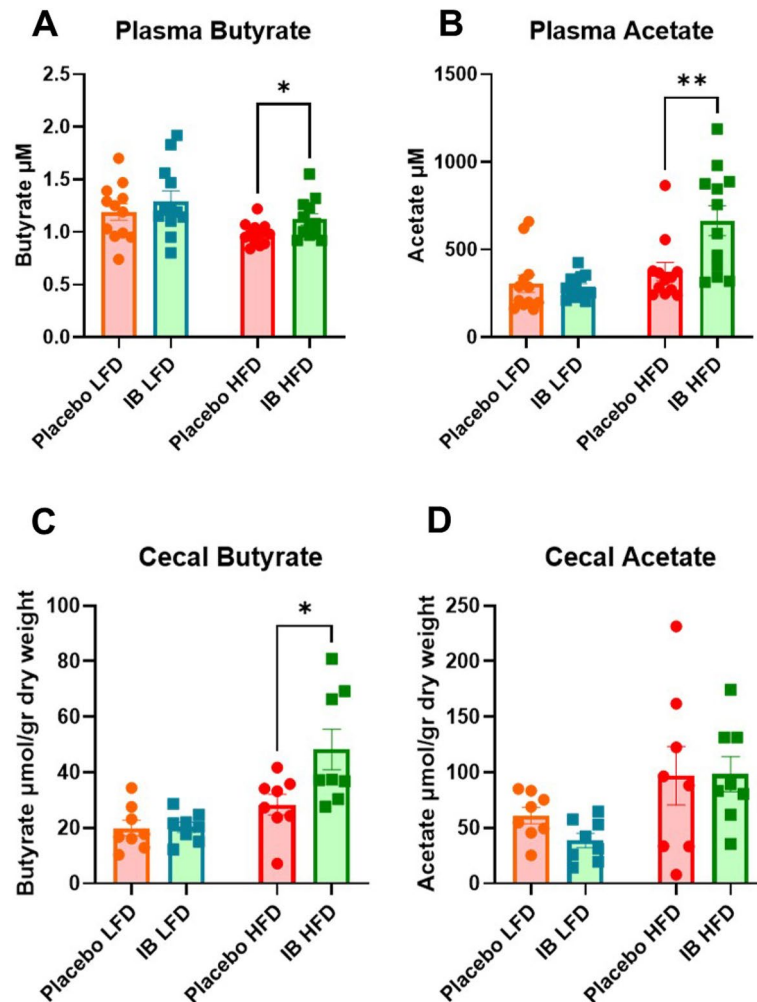


**Fig. 6** Circulating levels of bacterial SCFA and dietary fructoselysine. **A, B** Plasma concentrations of butyrate and acetate in mice. **C, D** Concentration of cecal butyrate and acetate in mice. All data are shown as mean values  $\pm$  SEM ( $N=12/\text{group}$ ). Mann–Whitney  $U$  test was used for statistical analysis. \* $P<0.05$ , \*\* $P<0.01$ . SCFAs and fructoselysine concentration were analyzed using LC–MS

IB ( $P=0.059$ , Supplementary Figure S4B). The increase in cecal butyrate levels after IB administration was more pronounced (28.4 versus 48.2,  $P=0.0281$ ), whereas cecal acetate levels were unchanged (Fig. 6C, D). More importantly, the significant increase of cecal butyrate after IB treatment was only found in HFD-treated mice but not in the LFD treatment groups (Fig. 6C), suggesting in vivo production of butyrate by IB, probably using fructoselysine as a source, as seen in the bacterial cultures (Fig. 2).

To exclude that the observed changes in gut-derived metabolites were due to alterations in gut barrier function, we also examined the expression in the small intestine and colon of genes encoding for tight junction molecules: claudin-4 (*Cldn4*), occludin (*Ocln*) and zona occludens-1 (ZO-1), *Tjp1* (tight junction protein 1) (Supplementary Figure S5A–F). At the protein level, occludin expression was significantly higher in lean IB-treated mice than in the placebo group (1,2 versus 5,2,  $P=0.0047$ ), whereas ZO-1 expression was unaltered by IB supplementation (Supplementary Figure S6A–C). These results indicate that IB did not have a negative effect on barrier integrity based on the expression of key epithelial tight junction proteins.

Taken together, these results highlight that the systemic effects of IB, observed in obese mice, are associated with the production of cecal butyrate and acetate, which are subsequently absorbed into the systemic circulation. The lack of changes in cecal and plasma butyrate and acetate in fed-LFD mice (Fig. 6A, B) suggests that the IB-associated cecal production of butyrate and acetate may have resulted from the higher fructoselysine content due to the high protein glycation in the HFD. Lastly, the beneficial effects observed so far seem to be determined only by the transit of exogenous IB through the intestinal tract rather than by the persistence of the given strain. We did not find an increase in the relative abundance of *Intestinimonas* in the fecal microbiota of the IB treatment groups as compared to placebo at the end of the study (Supplementary Figure S7A–B).

## Discussion

The Amadori product fructoselysine is abundant in processed foods, but only a small fraction of these protein-bound lysine Amadori products can be absorbed in the gut [3]. As a result, the majority of Amadori products are diverted to the lower gastrointestinal tract for microbial fermentation. We have previously demonstrated that *I. butyriciproducens* uniquely ferments fructoselysine to butyrate via the lysine and acetyl-CoA pathways simultaneously [12]. In the present study, we report three additional *Intestinimonas* isolates from human subjects, all of which have the ability to convert fructoselysine to butyrate and harbor all genes for a complete

fructoselysine pathway (Fig. 2). This indicates that *Intestinimonas* is a key player in the intestinal fructoselysine fermentation to butyrate and that *I. butyriciproducens* is the most abundant species within the *Intestinimonas* genus in the human gut, in good agreement with our previous report [23]. In addition, we isolated a new *Intestinimonas* species (AS-BT isolate) that shared many metabolic characteristics with *I. butyriciproducens*, except for the ability to synthesize pseudovitamin B12, an essential cofactor of lysine-5,6-aminomutase, a key protein involved in lysine/fructoselysine fermentation [36].

Interestingly, we found that the abundance of both *I. butyriciproducens* and fructoselysine pathway genes were negatively associated with several metabolic markers in a (pre-)diabetic cohort ( $n=1011$  subjects), suggesting a reduced capacity of the microbiome to convert fructoselysine to butyrate in cardiovascular and metabolically compromised subjects compared to healthy individuals. The reduced capacity of the human microbiota to convert fructoselysine to beneficial butyrate may lead to a higher fructoselysine accumulation and lower colonic butyrate levels, both of which are undesirable. While butyrate is required for a healthy colon, high levels of fructoselysine may facilitate its pH-driven conversion to  $\alpha$ -dicarbonyls and advanced glycation end products (AGEs), the levels of which have been associated with aging, atherosclerosis, and diabetes [37–40]. We have previously reported that the prevalence of *Intestinimonas* and fructoselysine fermentation genes were also associated with infant feeding modes [41]. In contrast, butyrate or short-chain fatty acids in general have been reported to be an important component in the control of body weight and insulin sensitivity [16]. This association from the cohort study is well in line with the results of the in vivo study, which showed that the administration of *I. butyriciproducens* GL3 strain (IB) exerts multiple metabolic benefits in diet-induced obesity. Indeed, bacterial supplementation led to significantly reduced body weight gain, iWAT accumulation, and fasting glucose levels in obese mice. In addition, following insulin administration, blood glucose levels remained lower in the IB-treated mice as compared to placebo. These effects were accompanied by increased IRS2 expression, enhanced expression of genes critical for lipid catabolism, and reduced inflammation in iWAT of IB-treated obese mice. Finally, bacterial administration resulted in higher levels of circulating and cecal butyrate.

Most of the observed IB-induced metabolic benefits in vivo are likely due to increased SCFA production by this commensal bacterium. Indeed, previous reports have shown that sodium butyrate administration limits weight gain, and improves glucose kinetics, insulin sensitivity, energy expenditure as well as mitochondrial function in

DIO mouse models [26, 34, 42]. Similarly, oral administration of sodium acetate was sufficient to counteract obesity, ameliorate insulin resistance, and increase energy expenditure and oxidative metabolism in DIO mice [34].

The short-chain fatty acid butyrate and acetate exert pleiotropic effects on the host by serving as an energy source (accounting for approximately 10 % of the caloric requirement in humans), functioning as histone deacetylase inhibitors, and signaling through host G protein-coupled receptors (GPRs) 41, 43 [43] and 109A/43 [44]. In addition to their protective effects against adiposity, SCFAs are also known to be anti-inflammatory molecules [13, 45–47]. In line with this, we found that the administration of the butyrate-producing strain *I. butyriciproducens* GL3 significantly reduced the production of TNF- $\alpha$ , IL-6, and IL-1 $\beta$  in iWAT. These effects are likely driven by SCFA-mediated inhibition of both the nuclear factor- $\kappa$ B (NF- $\kappa$ B) signaling and NLRP3 inflammasome activation [48–51]. Notably, both pathways are critical in the induction of meta-inflammation and obesity-induced insulin resistance [52, 53]. Accordingly, we observed that IB supplementation resulted in significantly lower fasting blood glucose levels and a trend toward improved glucose disposal upon insulin injection. Thus, the IB-induced improvement in glucose homeostasis may result from the inhibitory effects of SCFAs on local inflammation in iWAT and thus the maintenance of functional insulin signaling in adipocytes. Accordingly, we reported that the iWAT expression of *IRS2* was significantly increased upon IB administration as compared to placebo treatment. This effect is supported by previous reports demonstrating the ability of butyrate to increase the expression of the signaling molecules *IRS1* and *IRS2* [54], thereby facilitating insulin signaling.

Tissue inflammation and insulin resistance are closely linked to exacerbated intracellular lipid accumulation. In this regard, the transcriptional changes observed in iWAT upon bacterial treatment indicate an induction of fatty acid beta-oxidation via the PGC1- $\alpha$  and PPAR- $\alpha$  pathways which are master transcriptional regulators of mitochondrial biogenesis and oxidative metabolism [55]. The increased circulating levels of SCFAs found in IB-treated mice could explain the relatively lower iWAT weight with IB supplementation. Indeed, both in vitro and in vivo butyrate has been shown to activate the PGC1 $\alpha$  pathway and fatty acid oxidation pathway by increasing the CPT1 activity [26, 56, 57] as well as reducing adipocyte expansion [58]. As these are hypothetical pathways involved in lipid metabolism in IB-treated obese mice, we should be cautious in drawing conclusions because during the in vivo study we could not determine the activity levels of key enzymes and transcription factors, such as CPT1 $\alpha$  and PPARs, nor quantify the mitochondrial fatty

acid oxidation rates within the inguinal adipocytes. In addition, we have shown that IB administration results in local anti-inflammatory effects in iWAT, which are likely related to the reduced WAT depots. Consistent with the ability of butyrate to promote energy expenditure in vivo, the transcriptional signature of iWAT in IB-treated mice suggests the initiation of WAT browning/beiging. Yet protein expression could not confirm the occurrence of this process in all samples. Of note, the main effects of IB were detected in inguinal WAT rather than visceral (epididymal) WAT, a plausible explanation is that iWAT is more susceptible to modulations by external stimuli due to the higher expression of the browning markers *UCP1*, *Cidea*, and *Pdrn16*, as well as the beige markers *Tbx1* and *P2rx5* than eWAT at steady state [59].

Lastly, the observations that elevated plasma SCFA levels were found only in obese mice but not in lean mice following bacterial administration and the lack of differences in all measured clinical parameters between placebo- and IB-treated lean mice, underscore that the bacterial SCFA production is driven by the dietary differences. In fact, the high protein glycation in the HFD may lead to increased fructoselysine accumulation, thus providing additional sources for butyrate formation by *I. butyriciproducens*. Furthermore, the anti-inflammatory effects of *I. butyriciproducens* could be attributed, at least in part, to the utilization of a critical precursor, fructoselysine, of  $\alpha$ -dicarbonyls and AGEs, which are increased in type 2 diabetes and associated with diabetic complications by inducing oxidative stress and pro-inflammatory cytokine release [60–63]. Given that the mice were sacrificed after 6 h of fasting, i.e., thus during fructoselysine depletion, the observed significant increase in circulating and cecal butyrate levels may be an underestimate of the levels present in the fed state following bacterial administration.

Notably, the relative abundance of administered IB found in the feces was not increased by IB treatment; this could be explained by potential engraftment at a more proximal site in the gastrointestinal tract or by the inability of exogenous IB to stably engraft the colon due to competition with the endogenous *Intestinimonas* strains (detected at baseline). Nevertheless, the reported metabolic benefits together with the significant increase in butyrate concentrations, suggest that exogenous IB was metabolically active in the mouse intestine and that passage of IB may be sufficient to achieve metabolic improvements in DIO mice.

Overall, this study highlights the important role of the gut microbiota in regulating host physiology and particularly host metabolism and supports the development of microbiome-targeting approaches to prevent or

ameliorate metabolic disorders, such as obesity and type 2 diabetes.

## Conclusions

In summary, we found that *Intestinimonas* plays a key role in the conversion of dietary fructoselysine to butyrate in the gut and that *Intestinimonas butyriciproducens* abundance and fructoselysine pathway genes were negatively correlated with multiple risk biomarkers in a cohort study. In vivo, *I. butyriciproducens* counteracts adiposity, and improves glucose metabolism and tissue inflammation by converting dietary fructoselysine to butyrate and acetate in DIO mice.

## Material and methods

### Metagenomics analysis in the Swedish IGT cohort

The rarefied abundance levels of metagenomics species (CAG00017), annotated as *Intestinimonas butyriciproducens*, and 33 KEGG orthologies (KOs) involved in the fructoselysine metabolism were obtained from a previous study aiming to characterize the gut microbial changes in prediabetes and diabetes based on the Swedish IGT cohort ( $n=1011$ ) [20]. The relative differences of IB were then compared across individuals with distinct glucose intolerance levels versus the healthy control group. To examine the potential importance of fructoselysine metabolism to glucose intolerance, the relative abundances of each KO and/or the whole pathway (based on aggregated sum values of all KOs) were associated with 12 common clinical variables, such as the levels of fasting glucose, insulin, HbA1c, and triglycerides, indicative of the T2D status, respectively. The study was approved by the IRB of Sahlgrenska Hospital, Gothenburg University, and all subjects provided written informed consent.

### Isolation of *Intestinimonas* from human stool

Fresh fecal samples were collected in 15 ml falcon tubes containing anaerobic phosphate buffer (pH 7) and later stored in 25 % glycerol in 5 ml anaerobic bottles kept at  $-80^{\circ}\text{C}$  freezer. 0.5 ml of these fecal slurries was transferred to 10 ml anaerobic bicarbonate-buffered mineral salt medium (CP medium) containing 40 mM lysine as energy and carbon source to enrich lysine-fermenting bacteria. The headspace was filled with  $\text{CO}_2/\text{N}_2$  (1:4) at 1.5 atm and incubation was at  $37^{\circ}\text{C}$ . Subsequently, the enrichment cultures were transferred two more times in the same medium before being plated on YCFA agar medium containing 40 mM lysine as substrate (YCFA\_L). Single colonies were picked and plated at least 3 times on the same medium, which resulted in an axenic culture. The purity of the strains, designated as strain GL3, AS-BT, and IY4 was confirmed by 16S rRNA gene sequencing and microscopy. The strains were routinely

maintained in YCFA\_L medium at  $37^{\circ}\text{C}$ . 16S gene sequences of three isolates and strain AF211 were aligned with the multiple sequence aligner SINA [64] and merged with the Silva SSU Ref database (release 111). A phylogenetic tree of three isolates and *Intestinimonas* AF211 and closely related strains was constructed in the ARB software package (v. 6) by an algorithm [65].

Enrichment medium was done in an anaerobic bicarbonate-buffered mineral salt medium (CP medium) [66] consisting of ( $l^{-1}$ ): 0.53 g  $\text{Na}_2\text{HPO}_4 \cdot 2\text{H}_2\text{O}$ , 0.41 g  $\text{KH}_2\text{PO}_4$ , 0.3 g  $\text{NH}_4\text{Cl}$ , 0.11 g  $\text{CaCl}_2 \cdot 2\text{H}_2\text{O}$ , 0.10 g  $\text{MgCl}_2 \cdot 6\text{H}_2\text{O}$ , 0.3 g NaCl, 4.0 g  $\text{NaHCO}_3$  and 0.48 g  $\text{Na}_2\text{S} \cdot 9\text{H}_2\text{O}$  as well as alkaline and acid trace elements (each  $1\text{ ml } l^{-1}$ ) and vitamins ( $0.2\text{ ml } l^{-1}$ ) [66]. The alkaline trace element solution contained the following (mM): 0.1  $\text{Na}_2\text{SeO}_3$ , 0.1  $\text{Na}_2\text{WO}_4$ , 0.1  $\text{Na}_2\text{MoO}_4$ , and 10 NaOH. The acid trace element solution was composed of the following (mM): 7.5  $\text{FeCl}_2$ , 1  $\text{H}_3\text{BO}_3$ , 0.5  $\text{ZnCl}_2$ , 0.1  $\text{CuCl}_2$ , 0.5  $\text{MnCl}_2$ , 0.5  $\text{CoCl}_2$ , 0.1  $\text{NiCl}_2$  and 50 HCl. The vitamin solution had the following composition ( $g\ l^{-1}$ ): 0.02 biotin, 0.2 niacin, 0.5 pyridoxine, 0.1 riboflavin, 0.2 thiamine, 0.1 cyanocobalamin, 0.1 *p*-aminobenzoic acid and 0.1 pantothenic acid.

YCFA medium ( $l^{-1}$ ): 10 g soy peptone, 10 g yeast extract, 4 g  $\text{NaHCO}_3$ , 2.7 g sodium acetate, 4.5 g  $\text{K}_2\text{HPO}_4$ , 0.7 g  $\text{KH}_2\text{PO}_4$ , 0.9 g  $\text{NH}_4\text{Cl}$ , 0.9 g NaCl, 0.09 g  $\text{MgSO}_4$ , 0.09 g  $\text{CaCl}_2$ , 1 ml vitamin solution (1 mg biotin, 1 mg cobalamin, 3 mg PABA, 5 mg folic acid, 15 mg pyridoxamine in 100 ml  $\text{H}_2\text{O}$ ), 1 ml resazurine (0.5 g/l), 0.5 g L-cysteine. In case of agar medium, 10 g noble agar (DIFCO) was added to YCFA liquid before autoclave. The agar medium was then brought inside an anaerobic chamber and poured on agar plates. Those plates were then left slightly open for 30 min till the agar got dried. The plates were kept for a maximum a week in the chamber before use. All streaking and plating were performed in the anaerobic chamber while the plate incubation was done in anaerobic jars filled with  $\text{N}_2/\text{CO}_2$  in the gas phase by a gas exchange machine.

### Genome sequencing and fructoselysine pathway gene analysis

Strain GL3, IY4, and AS-BT were cultivated in 50 ml YCFA\_L liquid medium overnight at  $37^{\circ}\text{C}$ . The bacterial cells were harvested at the late exponential phase by centrifuging at 4700 rpm at  $4^{\circ}\text{C}$ . The cell pellets were used for DNA extraction using MasterPure™ Gram Positive DNA Purification Kit (Epicentre) according to the manufacturer's instructions. After checking the quality on a Nanodrop, 30  $\mu\text{l}$  of high-quality DNA solution was sent in dry ice to GATC for draft genomes using Illumina sequencing technology. Draft genome assemblies were constructed using the MyPro assembly pipeline [67]. Raw

reads were quality-checked using FastQC [68, 69]. Reads were trimmed and subsampled to a total coverage of  $100\times(50\times$  for forward reads,  $50\times$  for reverse reads), then assembled using 4 different assembly tools: VelvetOptimiser [70], Edena [71], SOAPdenovo [72] and SPAdes [73]. The resulting contigs were ordered with r2cat [74] using the *Intestinimonas butyriciproducens* AF211 genome (CP011307) as a reference and overlapping contigs merged resulting in the final genome assembly. Genome assemblies were then annotated using RAST [75]. The annotation was done by RAST server [75]. Functional prediction of proteins was verified manually by BLASTing the amino acid sequences in Pfam [76], Brenda, Interpro [77], and Uniprot databases. In addition, the screening of antibiotic resistance genes was done using ABRICATE against the NCBI, ARG-ANNOT, ResFinder, and VFDB databases.

#### Fructoselysine growth experiment

Conversion of fructoselysine was tested in CP medium containing 5 mM fructoselysine (provided by TRC, North York, Canada). The inoculum was 2.5 % from active cultures of strain GL3, IY4, AS-BT, and AF211 for the growth test. All strains were pre-cultured in YCFA containing 20 mM lysine. The bacterial cultures were sampled during the growth up to 48 h for substrate and end metabolite measurements as described below.

#### Antibiotic resistance profile

The E-test was done to identify minimal inhibitory concentrations (MICs) according to the manufacturer's protocol (bioMérieux, France). Both strains were pre-grown in RCM broth (overnight cultures) and 50  $\mu$ l was spread on RCM agar plates (1.5 % w/v agar) until the agar surface was dry and the liquid was absorbed by the agar. Two E-test strips were used per antibiotic and considered duplicates. Antibiotics tested included ciprofloxacin, cefotaxime, erythromycin, oxacillin, teicoplanin, tetracycline, tobramycin, vancomycin, and sulfamethoxazole. The concentration range was 0.016–256  $\mu$ g/ml for chloramphenicol, oxacillin, tetracycline, tobramycin, and vancomycin, and 0.016–32  $\mu$ g/ml for ciprofloxacin, cefotaxime, erythromycin, teicoplanin and sulfamethoxazole. MIC values were recorded directly from the strips after 24 h, 48 h, and rechecked after 4 days.

As tetW gene was detected in the genomes of most *Intestinimonas* strains and some of *Intestinimonas* strains were found to be resistant in erythromycin from the Etest, tetracycline and erythromycin were selected to perform the MIC test in liquid according to EFSA guideline. The test was done in 10 ml YCFA medium containing lysine as substrate in anaerobic bottles filled with  $\text{CO}_2/\text{N}_2$  (1:4) at 1.5 atm. The concentration of

tetracycline was twofold reduction in each bottle from 256 to 1  $\mu$ g/ml. The 256  $\mu$ g/ml tetracycline bottle was prepared in a 20 ml growth medium by adding 1 ml of tetracycline filter-sterilized stock solution (5.12 mg/ml) to a 19 ml complete medium. This medium was then serially diluted two-fold to get concentrations of 128, 64, 32, 16, 8, 4, 2, and 1  $\mu$ g/ml. All these bottles were inoculated 2 % with an overnight culture. The growth was monitored by OD measurement at 24 h, 48 h, 72 h, and 96 h. Bottles without tetracycline were used as a positive control. MIC test for erythromycin in liquid was done in the same way by replacing tetracycline with erythromycin.

#### Animal studies

All animal studies were approved by the Institute Ethical Committee. C57BL6/J male mice were purchased from Charles River at the age of 4 weeks, fed a regular chow diet and kept under regular 12 h/12 h light/dark cycles. Mice were acclimatized for at least 1 week prior to the start of the animal study. To determine the impact of IB on whole-body metabolism, male mice were randomized in 4 groups ( $N=12$ ) receiving 3 times/week  $2\times 10^9$  CFU *Intestinimonas butyriciproducens* GL3 or placebo solution (anaerobic PBS) by oral gavage and fed ad libitum a low-fat diet (LFD, 10 %kcal from fat, Research Diets, D12450ji) or high-fat diet (HFD, 60 %Kcal from fat, Research Diets, D12492i). The in vivo study lasted for 14 weeks: mice were fed LFD/HFD for 13 weeks and IB/placebo supplementation started 1 week before switching to special diets. To minimize cage effects on the microbiota composition and avoid fighting between cohoused male mice, 3 mice were housed in one cage [78]. Body weight and food consumption were monitored once a week. At the end of the study, insulin-tolerance test (ITT) was performed in obese mice on HFD: after 6-h fasting, mice received an intraperitoneal injection of insulin (0.5 U/kg); blood glucose levels were assessed by tail prick using glucometer strips at 0, 15, 30, 45, 60 and 90 min post-injection. To avoid unnecessary discomfort and suffering due to potential hypoglycemic events, lean mice fed a LFD were not subjected to ITT. Mice were sacrificed under anesthesia (5 % isoflurane,  $\text{O}_2$  flow of 2 L/min), blood was collected by cardiac puncture, and harvested organs were stored in formalin (for later paraffin-embedding) and snap-frozen in liquid nitrogen. White-adipose tissues were weighed immediately after collection.

#### Targeted liquid chromatography tandem mass spectrometry

##### Protein-bound fructoselysine in the two diets

Protein-bound fructoselysine in the two diets was indirectly quantified through furosine upon acidic hydrolysis

according to the method of Troise et al. [71]. A Nexera U-HPLC system coupled with a LCMS-8050 triple quadrupole mass spectrometer (Shimadzu Corporation, Kyoto, Japan) was used and for the separation of furosine and its internal standard d4-furosine, a core-shell Kinetex HILIC column (2.6  $\mu\text{m}$ , 2.1 mm  $\times$  100 mm, Phenomenex) was thermostated at 30  $^{\circ}\text{C}$ , with a flow rate of 0.4 mL/min. The mobile phases consisted of 0.1 % formic acid (solvent A), 0.1 % formic acid in acetonitrile (solvent B), and 50 mmol/L ammonium formate (solvent C). Positive ionization multiple reaction monitoring (MRM) mode was used, and profile data were acquired and analyzed through LabSolutions (Shimadzu Corporation).

#### **Free fructoselysine and SCFA in the growth medium, mouse caecum, and plasma samples**

Fructoselysine, lysine, and SCFAs in CP medium and mice caecum were analyzed by liquid chromatography high-resolution tandem mass spectrometry (LC-MS/MS) by means of a Vanquish Core LC system interfaced to an Exploris 120, hybrid quadrupole Orbitrap mass spectrometer (Thermo Fisher Scientific, Bremen, Germany). For fructoselysine and lysine quantification in the CP medium, samples were diluted in a solution acetonitrile/water (50:50, v/v) according to the linearity range used for the calibration curve. For fructoselysine quantification in caecum and plasma, the analytical protocol was adapted from Wolf et al. [7], with minor modifications. Briefly, 20  $\mu\text{L}$  of plasma or 20  $\mu\text{L}$  of caecum supernatants were diluted in ice-cold methanol (ratio 1:3). Suspensions were centrifuged at 18,000  $\times g$  for 10 min, 4  $^{\circ}\text{C}$  and 50  $\mu\text{L}$  were dried under vacuum in a centrifugal evaporator (Savant, Thermo Fisher Scientific). Dried samples were resuspended in a solution consisting of 50 % acetonitrile in water. Lysine and its Amadori compound were separated at 35  $^{\circ}\text{C}$  through a zwitterionic sulfobetaine column (Atlantis Premier BEH, Z-HILIC, 100  $\times$  2.1, 1.7  $\mu\text{m}$ , Waters, Milford, MA) with the following gradient of solvent B (minutes/%B): (0/5), (1/5), (2/50), (6/50). Mobile phases consisted of 0.1 % formic acid in acetonitrile (solvent A) and 0.1% formic acid in water (solvent B) and the flow rate was 0.2 mL/min. The analyzer resolution was set at 60,000 (FWHM at  $m/z$  200), fructoselysine and lysine were identified and quantified in product ion scan positive mode screening the precursor ions ( $\text{C}_{12}\text{H}_{24}\text{N}_2\text{O}_7$   $[\text{M}+\text{H}]^+$  309.1656, for fructoselysine and  $\text{C}_6\text{H}_{14}\text{N}_2\text{O}_2$   $[\text{M}+\text{H}]^+$  147.1128 for lysine) and monitoring for both fructoselysine and lysine the characteristic fragment ion at  $m/z$  84.0808. A linear calibration curve was built in the range 100–10,000 nM and the concentration reported in mM was measured through the standard addition technique by using CP medium, caecum, or plasma as blank samples.

For acetate, butyrate, and isobutyrate separation in CP growth experiments, supernatants were directly diluted in o-phosphoric acid (0.5 % final concentration in water, 1:10, v:v), while for mice caecum content, samples were centrifuged at 4  $^{\circ}\text{C}$ , 18,000  $\times g$  for 15 min and supernatants diluted 1:10 v/v in 0.5 % o-phosphoric acid. Samples were centrifuged at 18,000  $\times g$  before transferring clear supernatants to a glass vial. Analytes were separated through a graphite column thermostated at 40  $^{\circ}\text{C}$  (Hypercarb, 100  $\times$  1.0, 1.7  $\mu\text{m}$ , Thermo Fisher Scientific) with the following gradient of solvent B (minutes/%B): (0/0), (2/0), (6/75), (8/75). Mobile phases consisted of 0.1% formic acid in water (solvent A) and 0.1 % formic acid in acetonitrile (solvent B) and the flow rate was 0.1 mL/min. H-ESI parameters were as follows: static spray voltage 3.2 kV, ion transfer tube, and vaporizer temperature were both at 280  $^{\circ}\text{C}$ ; sheath gas flow and auxiliary gas flow were 35 and 7 arbitrary units. Acetate and butyrate were quantified in full MS scan positive ion mode screening the two precursor ions ( $\text{C}_2\text{H}_4\text{O}_2$   $[\text{M}+\text{H}]^+$  61.0284 and  $\text{C}_4\text{H}_8\text{O}_2$   $[\text{M}+\text{H}]^+$  89.0597) with a mass accuracy below 3 ppm. A linear calibration curve was built in the range of 0.5–10 mM by using acetate and butyrate as internal standards and concentration reported in mM. Profile data were collected using Xcalibur 4.5 (Thermo Fisher Scientific, Waltham, MA) and fragmentation spectra were recorded by using Free Style software (v. 1.8, Thermo Fisher Scientific, Waltham, MA, USA). Analytical performance robustness, sensitivity, reproducibility, repeatability, linearity, accuracy, carry over and matrix effects were evaluated through authentic analytical standards in the Trace Finder environment (v. 5.1, Thermo Fisher Scientific, Waltham, MA, USA).

SCFA concentration in mouse plasma samples was quantified according to the procedure detailed by Mazzoli et al. [78] with minor modifications. Briefly, 10  $\mu\text{L}$  of plasma were spiked with 1  $\mu\text{L}$  of  $^{13}\text{C}$ -SCFA internal standard mix (final concentration 0.1 mM for each carbon labeled compound). Upon protein precipitation, suspensions were derivatized with 60  $\mu\text{L}$  of 3-nitrophenylhydrazine (200 mM) and 10  $\mu\text{L}$  of N-(3-dimethylaminopropyl)-N'-ethylcarbodiimide (EDC, 120 mM in 6 % pyridine). The derivatization reaction was stopped with the addition of 10  $\mu\text{L}$  quinic acid (200 mM) and incubation under shaking at room temperature for 15 min. Samples were centrifuged and supernatants were diluted up to 1 mL with 10:90 methanol:water solution (v/v). Hydrazone derivative quantitation was achieved by a U-HPLC system (Ultimate 3000 RS, Thermo Fisher Scientific) interfaced to a linear ion trap hybrid Orbitrap high-resolution mass spectrometer (LTQ Orbitrap XL, Thermo Fisher Scientific). Chromatographic separation included a reversed-phase C18 column thermostated at 40  $^{\circ}\text{C}$  (Kinetex C18 PS, 100  $\times$  2.1 mm, 2.6  $\mu\text{m}$ ,

Phenomenex, Torrance, CA, USA) with the following gradient of solvent B (minutes/%B): (0/5), (5/5), (12.3/35), (13.3/85), (14/99), (16/99). Mobile phases consisted of water (solvent A) and acetonitrile (solvent B) and the flow rate was 0.2 mL/min. LC stream was interfaced to an electrospray ion source (ESI) working in negative ion mode scanning the ion in the  $m/z$  range 100–400 with a capillary temperature was 300 °C. Analytes profile data in full MS mode were collected using Xcalibur 2.1 (Thermo Fisher Scientific). The calibration curve was performed by internal standard technique in the linearity range 1–1000  $\mu\text{M}$  by using the same procedure detailed above for plasma samples. Analytical performances for the three procedures are detailed in Supplementary Table S6.

#### RNA isolation

RNA was isolated from iWAT tissues, which were stored at 80 °C until analysis, using standard RNA isolation protocol. In short, biopsies were mixed with 1 ml TriPure (Roche) and homogenized using a ceramic beads homogenizer. After adding 0.2 ml chloroform to 1 ml Tripure solution, samples were centrifuged (15 min, 12,000 $\times$ g, 4 °C). The aqueous phase was transferred and mixed with 0.5 ml isopropanol and centrifuged (15 min, 12,000 $\times$ g, 4 °C). Afterwards, the pellets were resuspended in 1 ml of 70 % ethanol and centrifuged (15 min, 7500 $\times$ g, 4 °C). RNA was eluted in 20  $\mu\text{l}$  RNase free water. RNA concentrations were measured using the NanoDrop 1000 (Thermo Scientific).

#### DNA isolation from mouse fecal samples

Mouse fecal samples were lysed in Lysing Matrix E tubes (MP Biomedicals) containing ASL buffer (Qiagen). Samples were lysed after homogenization by 2 min vortexing with subsequent two heating cycles at 90 °C for 10 min followed by three bead beating bursts at 5.5 m s<sup>-1</sup> for 60 s in a FastPrep-24 instrument (MP Biomedicals). Samples were cooled on ice after each bead-beating burst for 5 min. The fecal DNA supernatants were collected after two centrifugation cycles at 4 °C. Supernatants of the centrifugation steps were pooled, and aliquots of 600  $\mu\text{L}$  from each sample were purified with the QIAamp DNA Mini kit (QIAGEN) in the QIAcube instrument (QIAGEN). Finally, DNA was eluted in 200  $\mu\text{L}$  of AE buffer (10 mM Tris-CL, 0.5 mM EDTA, pH 9.0).

#### Real time quantitative polymerase chain reaction (RT-qPCR)

For analysis of gene expression in mouse tissues harvested at the end of the animal study, 1  $\mu\text{g}$  of RNA was converted to cDNA with SensiFAST cDNA synthesis kit (Meridian Bioscience) according to the manufacturer's instructions. qPCR was performed on a CFX Opus 384

PCR machine (BioRad) using SensiFAST SYBR No-ROX Green (Meridian Bioscience). The following QPCR program was used: 10 min at 95 °C, followed by 45 cycles of 15 s at 95 °C for denaturation, 30 s at 60 °C for annealing and elongation, and melting curve (65 to 95 °C at an increment of 0.5 °C/5 s).

Gene expression was normalized with the expression of the housekeeping gene *Hprt*; relative gene expression was calculated with the “delta Ct” method and shown as 2<sup>-delta Ct</sup>. In order to assess the relative abundance of *Intestinimonas* in feces, samples were brought to a DNA concentration of 5 ng/ $\mu\text{l}$  and the set of universal primers BAC1396 and PROK1492R and of PFF590f and PFF702r [12] were used to quantify, respectively, total bacteria and *Intestinimonas*. Data are shown as a percentage of total bacteria in feces. The following PCR program was used: 10 min at 95 °C, followed by 40 cycles of 15 s at 95 °C denaturation, 30 s at 60 °C annealing, 45 s at 72 °C elongation, and ending with melting curve (60 to 95 °C at an increment of 0.5 °C every 5 s). All primers were manufactured by Sigma-Aldrich; primer sequences are provided in Supplementary Table S7.

#### Western blotting

iWAT tissues were lysated in RIPA buffer (Thermo Fisher Scientific) containing protease and phosphatase inhibitors (cOmplete™ Protease inhibitor and PhosSTOP Phosphatase Inhibitor Cocktails, Sigma) using a ceramic beads homogenizer. After centrifugation, the lipid layer was removed and protein concentration was determined by BCA assay (Thermo Fisher Scientific).  $\beta$ -mercaptoethanol was added as a reducing agent to sample lysates. Samples were loaded on 4–12% NuPage Bis-Tris polyacrylamide gels (Invitrogen). Proteins were transferred to PVDF membranes (BioRad), which were blocked in 5 % milk in TBS-T (Tris Buffered Saline-Tween-20). Membranes were incubated overnight at 4 °C with primary antibodies: rabbit antibodies anti-IRS2, anti-UCP1, anti-alpha-tubulin (Cell Signaling), anti-PGC1 alpha, anti-CPT1A, anti-PRDM16 (Abcam), anti-ZO-1 (ThermoFisher). Horseradish peroxidase (HRP)-conjugated secondary antibodies (polyclonal goat anti-rabbit IgG or monoclonal goat anti-mouse IgG, Dako, 1:3000) were incubated for 1 h at room temperature. HRP activity was visualized with peroxidase substrate for enhanced chemiluminescence and imaged with ChemiDoc MP Imaging System (BioRad). Densitometric quantification analysis was performed using the ImageJ software. All protein levels were normalized to the loading control ( $\beta$ -actin or  $\alpha$ -tubulin).

#### ELISA

Sections of frozen iWAT tissues were cut and homogenized in 400  $\mu\text{l}$  RIPA buffer (Thermo Fisher Scientific)

containing protease and phosphatase inhibitors (cOmplete™ Protease inhibitor and PhosSTOP Phosphatase Inhibitor Cocktails, Sigma) using a ceramic beads homogenizer. Protein concentration was determined with BCA assay (Thermo Fisher Scientific). The tissue concentrations of TNF- $\alpha$ , IL-6, and IL-1 $\beta$  cytokines were quantified using respectively the mouse TNF $\alpha$ /IL-6 DuoSet ELISA (R&D Systems) and ELISA MAX™ Deluxe Set Mouse IL-1 $\beta$  (BioLegend) according to the manufacturers' protocol. The absorbance was measured at an optical density (OD) of 450 nm and 570 nm using the Tunable Microplate Reader VersaMax (Molecular Devices, USA). The cytokine levels were normalized for protein concentrations.

### Histology and immunohistochemical staining

Tissues were fixed in 10 % buffered formalin overnight, dehydrated in 70 % ethanol, and embedded in paraffin. Sections of 4  $\mu$ m were cut and stained for macrophage marker F4/80. Formalin-fixed paraffin-embedded (FFPE) sections were deparaffinized in 100 % xylene and rehydrated in ethanol (100 %, 96 %, and 70 %) and H<sub>2</sub>O, followed by a block of endogenous peroxidase in 3 % H<sub>2</sub>O<sub>2</sub> methanol for 20 min and heat-induced epitope retrieval (HIER) in citrate buffer pH 6.0 at 100 °C for 10 min. iWAT sections were incubated with the following antibodies: FITC anti-mouse F480 (BioLegend) diluted 1:5000 for 2 h at room temperature, rabbit anti-FITC (Bio-Rad) diluted 1:1000 for 1 h at room temperature, finally BrightVision Poly-HRP-conjugates goat anti-rabbit IgG (ImmunoLogic) diluted 1:2 for 30 min at room temperature. Staining was visualized with 3,3 Diaminobenzidine (DAB) kit (Sigma Aldrich) and counterstaining was performed using hematoxylin. Per sections, 10 pictures were captured at random using a Leica MC170 HD stand-alone microscope camera (Danaher Corporation, USA). Subsequently, analysis of the digital images was conducted using ImageJ software.

### Statistical analysis of the in vivo data

Statistical differences between the placebo and IB-treated groups were assessed using Mann Whitney test, and the differences were considered statistically significant with *P* values < 0.05.

### Abbreviations

IB	<i>Intestinimonas butyriciproducens</i> GL3
FL	Fructoselysine
AGE	Advanced glycation end products
SCFA	Short chain fatty acid
WAT	White adipose tissue
eWAT	Epididymal white adipose tissue
iWAT	Inguinal white adipose tissue
T2D	Type 2 diabetes
IFG	Impaired fasting glucose

IGT	Impaired glucose tolerance
CGI	Combined glucose intolerance
IrNGT	Low-risk normal glucose tolerance
BMI	Body mass index
MIC	Minimum inhibitory concentration
DIO	Diet-induced obesity
HFD	High-fat diet
LFD	Low-fat diet
AUC	Area under the curve
IPITT	Intraperitoneal insulin tolerance test
IrS2	Insulin receptor substrate 2
Ppargc1a4	Peroxisome proliferator-activated receptor gamma coactivator 1-alpha
Ppara	Peroxisome proliferator-activated receptor- $\alpha$
Cpt1a	Carnitine palmitoyl transferase 1- $\alpha$
Ucp1	Uncoupling protein 1
Cidea	Cell death-inducing DFFA Like Effector A
Prdm16	PR domain containing 16
Dio2	Iodothyronine deiodinase 2
Tbx1	T-box protein 1
TNF- $\alpha$	Tumor necrosis factor-alpha
IL-6	Interleukin-6
IL-1 $\beta$	Interleukin-1 beta

### Supplementary Information

The online version contains supplementary material available at <https://doi.org/10.1186/s40168-024-02002-9>.

Supplementary Material 1. Supplementary Figure S1: (A) Concentrations of protein-bound fructoselysine measured in standard chow diet and high-fat diet (HFD). Concentrations in diet shown as ratios of mg protein-bound fructoselysine per 100g of dietary proteins. Data are shown as mean values  $\pm$  SEM (*N* = 3/group), \*\*\*\* *P* < 0.001. Fructoselysine concentrations were analyzed using LC-MS/MS. A detailed detection method is described in the Methods section. Supplementary Figure S2: (A-D) Protein expression of PGC1 $\alpha$ , CPT1A, UCP1 and PRDM16 in inguinal WAT of DIO mice analyzed by western blotting. (E) Images of the western blots performed on 8 samples from HFD placebo group and 8 samples from the HFD IB group. Supplementary Figure S3: (A-F) Expression levels of genes encoding molecules involved in mitochondrial metabolism, lipid metabolism and mitochondrial uncoupling in brown adipose tissue samples. Data analyzed by Mann-Whitney U test. *Ppargc1a4* (Peroxisome proliferator-activated receptor gamma coactivator 1-alpha), *Ppara* (Peroxisome proliferator-activated receptor alpha), *Pparg1* (Peroxisome proliferator-activated receptor gamma 1), *Cpt1a* (Carnitine palmitoyltransferase 1A), *Ucp1/2* (Uncoupling protein) 1/2. Supplementary Figure S4: (A) Plasma concentrations of fructoselysine and (B) ratios of plasma butyrate / fructoselysine in mice. All data are shown as mean values  $\pm$  SEM (*N* = 12/group). Mann-Whitney U test was used for statistical analysis. SCFAs and fructoselysine concentrations were analyzed using LC-MS/MS. Supplementary Figure S5: (A-F) Expression levels of genes encoding critical molecules for intestinal barrier function in (A-C) the small intestine and (D-F) the colon. Differences between placebo and IB groups analyzed with Mann-Whitney U test. All data are shown as mean values  $\pm$  SEM (*N* = 12/group). *Cldn4* (Claudin-4), *Ocln* (Occludin), *Tjp1* (Zona occludens 1). Supplementary Figure S6: (A-B) Quantification of tight-junction protein expression in small intestinal samples from placebo and IB-treated mice fed LFD or HFD. Expression normalized to the level of alpha-tubulin. (C) Images of westernblots used to analyze the protein expression of occludin and ZO-1 in 8 samples per treatment group. Differences between placebo and IB groups analyzed with Mann-Whitney U test. All data are shown as mean values  $\pm$  SEM (*N* = 12/group); \*\* *P* < 0.01. Supplementary Figure S7: Relative abundance of *Intestinimonas* detected in mouse feces as compared to total bacteria detection by qPCR method at baseline (A) and at the end of the study (B). All data are shown as mean values  $\pm$  SEM (*N* = 12/group); Supplementary Table S1: Grouping of genes for individual metabolism. Supplementary Table S2: Fructoselysine pathway genes found in genomes of four *Intestinimonas* strains. + : presence; - : absence. Supplementary Table S3: Genes involved in pseudovitaminB12 synthesis in 4 *Intestinimonas* strains. + :

presence;-: absence. Supplementary Table S4: Antibiotic resistance profiles of 4 *Intestinimonas* strains. Minimal inhibitory concentrations are indicated ( $\mu\text{g/ml}$ ). Supplementary Table S5: Numbers of resistance genes detected in the genomes of four *Intestinimonas* strains (AF211, AS-BT, IY4 and GL3). Supplementary Table S6: Elemental composition and retention time of the analytes quantified through the three procedures described in material and methods section, HILIC-MS/MS for lysine and fructoselysine, reversed phase (RP) LC-MS/MS upon derivatization for SCFA in plasma, LC-MS/MS for SCFA in fecal supernatants (PGC); in bold internal standard used for quantification and recovery of the derivatization procedure. Error ( $\Delta$  ppm) was calculated as the ratio between the difference of the theoretical mass minus the experimental mass and the theoretical mass, multiplied per one million. In the case of reversed phase (RP), each compound is intended as hydrazone derivative and reported in italic. For porous graphite column (PGC), target analytes were detected and quantified in their native form without any derivatization. Supplementary Table S7: primer sequences for assessing the expression of transcripts by qPCR in mouse tissues.

### Acknowledgements

We thank prof. Willem M. DeVos and Dr. Jos Seegers for valuable discussions for this work.

### Authors' contribution

TPNB and ER conceptualized and designed the study. HW did metagenomic analysis. TPNB performed culturing, isolation and genomic analysis. ER and NR, SH, JA performed the animal work, performed ex vivo measurement and analyzed the data. ADT, VF, AS and SDP performed extraction and measurements of fructoselysine and SCFAs in cecum content and plasma samples. SG produced the bacteria for the animal work. TPNB, ER, and NR are major contributors in writing the manuscript. All authors read and approved the final manuscript.

### Funding

The work is partially funded by the Euro-Trans-Bio grant HBC.2017.0100 for the DM Prevent-project. TPNB is supported by an NWO VENI grant and Amsterdam UMC bridging grant. ER and NR are supported by an NWO VIDI grant and AUMC Starter grant (appointed to ER). MN is supported by a personal ZONMW-VICI grant 2020 (09150182010020) and an ERC-Advanced Grant 2023 FATGAP (101141346). ADT, SDP, and AS research was partially funded by the National Recovery and Resilience Plan, mission 4, component 2, investment 1.3, call n. 341/2022 of the Italian Ministry of University and Research funded by the European Union-NextGenerationEU for the project "ON Foods-Research and innovation network on food and nutrition Sustainability, Safety and Security-Working ON Foods"; project PE00000003, concession decree n. 1550/2022, CUP B83C22004790001.

### Availability of data and materials

The human metagenomic data from the human cohort have been deposited in EGA as previously published [16], ref 16:Wu, H., et al., The Gut Microbiota in Prediabetes and Diabetes: A Population-Based Cross-Sectional Study, *Cell Metabolism*, 2020. 32(3): p. 379-390.e3.

### Declarations

#### Ethics approval and consent to participate

The human work protocol was approved by the Ethics Review Board in Gothenburg as previously indicated [20]. All animal experiments were conducted according to the 'Guide to the Care and Use of Experimental Animals' approved by the Ethics Committee on Animal Care and Use in Academisch Medisch Centrum, the Netherlands.

Fresh stools for bacterial isolation work were collected from two healthy donors of whom informed consents were obtained following Good Clinical Practice.

#### Consent for publication

Not applicable.

#### Competing interests

M.N. is co-founder and member of the Scientific Advisory Board of Caelus Pharmaceuticals and Advanced Microbial Interventions, the Netherlands. However,

none of these possible conflicts of interest bear direct relations to the outcomes of this specific study. The other authors declare no competing interests.

### Author details

<sup>1</sup>Department of Experimental Vascular Medicine, Amsterdam UMC, Amsterdam, the Netherlands. <sup>2</sup>Amsterdam Institute for Immunology and Infectious Diseases, Amsterdam, the Netherlands. <sup>3</sup>Proteomics, Metabolomics & Mass Spectrometry Laboratory, Institute for the Animal Production System in the Mediterranean Environment, National Research Council, 80055 Portici (Naples), Italy. <sup>4</sup>State Key Laboratory of Genetic Engineering, School of Life Sciences, Fudan Microbiome Center, and Human Phenome Institute, Fudan University, Shanghai 200438, China. <sup>5</sup>Caelus Pharmaceuticals, Amsterdam, the Netherlands. <sup>6</sup>The Wallenberg Laboratory, Department of Molecular and Clinical Medicine, Sahlgrenska Academy, University of Gothenburg, Bruna Stråket 16, 41345 Gothenburg, Sweden. <sup>7</sup>Department of Food Quality and Design, Wageningen University, Wageningen, the Netherlands. <sup>8</sup>Laboratory of Microbiology, Wageningen University, Wageningen, the Netherlands.

Received: 29 May 2024 Accepted: 10 December 2024

Published online: 20 January 2025

### References

- Fujisaka S, et al. Diet, genetics, and the gut microbiome drive dynamic changes in plasma metabolites. *Cell Rep*. 2018;22(11):3072–86.
- Corbin KD, et al. Host-diet-gut microbiome interactions influence human energy balance: a randomized clinical trial. *Nat Commun*. 2023;14(1):3161.
- Erbersdobler HF, Faist V. Metabolic transit of Amadori products. *Food / Nahrung*. 2001;45(3):177–81.
- Tuohy KM, et al. Metabolism of maillard reaction products by the human gut microbiota – implications for health. *Mol Nutr Food Res*. 2006;50(9):847–57.
- Henning C, Glomb MA. Pathways of the Maillard reaction under physiological conditions. *Glycoconj J*. 2016;33(4):499–512.
- de Courten B, et al. Dietary advanced glycation end products consumption as a direct modulator of insulin sensitivity in overweight humans: a study protocol for a double-blind, randomized, two period cross-over trial. *JMIR Res Protoc*. 2015;4(3):e93.
- Uribarri J, et al. Diet-derived advanced glycation end products are major contributors to the body's AGE pool and induce inflammation in healthy subjects. *Ann N Y Acad Sci*. 2005;1043(1):461–6.
- Luévano-Contreras C, et al. Dietary advanced glycation end products and cardiometabolic risk. *Curr Diab Rep*. 2017;17(8):63.
- Filipp L, et al. Metabolization of the Amadori Product N-ε-Fructosyllysine by Probiotic Bacteria. *J Agric Food Chem*. 2024;72:2718–26.
- Wiame E, et al. Identification of a pathway for the utilization of the Amadori product Fructoselysine in *Escherichia coli*. *J Biol Chem*. 2002;277(45):42523–9.
- Wolf AR, et al. Bioremediation of a Common Product of Food Processing by a Human Gut Bacterium. *Cell Host Microbe*. 2019;26(4):463–477.e8.
- Bui TPN, et al. Production of butyrate from lysine and the Amadori product fructoselysine by a human gut commensal. *Nat Commun*. 2015;6:10062.
- Chang PV, et al. The microbial metabolite butyrate regulates intestinal macrophage function via histone deacetylase inhibition. *Proc Natl Acad Sci*. 2014;111(6):2247–52.
- Furusawa Y, et al. Commensal microbe-derived butyrate induces the differentiation of colonic regulatory T cells. *Nature*. 2013;504:446.
- Archer S, et al. p21(WAF1) is required for butyrate-mediated growth inhibition of human colon cancer cells. *Proc Natl Acad Sci U S A*. 1998;95:6791–6.
- Canfora EE, Jocken JW, Blaak EE. Short-chain fatty acids in control of body weight and insulin sensitivity. *Nat Rev Endocrinol*. 2015;11:577–91.
- Udayappan S, et al. Oral treatment with *Eubacterium hallii* improves insulin sensitivity in db/db mice. *NPJ Biofilms Microbiome*. 2016;2:16009.
- Giljiamse PW, et al. Treatment with *Anaerobutyricum soehngenii*: a pilot study of safety and dose-response effects on glucose metabolism in human subjects with metabolic syndrome. *NPJ Biofilms Microbiomes*. 2020;6(1):16.

19. Kootte RS, et al. Improvement of insulin sensitivity after lean donor feces in metabolic syndrome is driven by baseline intestinal microbiota composition. *Cell Metab.* 2017;26(4):611–619.e6.
20. Wu H, et al. The Gut Microbiota in Prediabetes and Diabetes: A Population-Based Cross-Sectional Study. *Cell Metab.* 2020;32(3):379–390.e3.
21. Miller KA, et al. A mannose family phosphotransferase system permease and associated enzymes are required for utilization of fructoselysine and glucoselysine in *Salmonella enterica* Serovar Typhimurium. *J Bacteriol.* 2015;197(17):2831–9.
22. Kläring K, et al. *Intestinimonas butyriciproducens* gen. nov., sp. nov., a butyrate-producing bacterium from the mouse intestine. *Int J Syst Evol Microbiol.* 2013;63(Pt 12):4606–12.
23. Bui TPN, et al. Comparative genomics and physiology of the butyrate-producing bacterium *Intestinimonas butyriciproducens*. *Environ Microbiol Rep.* 2016;8(6):1024–37.
24. Lee K, et al. Population-level impacts of antibiotic usage on the human gut microbiome. *Nat Commun.* 2023;14(1):1191.
25. Kruse T, et al. vanI: a novel d-Ala-d-Lac vancomycin resistance gene cluster found in *Desulfitobacterium hafniense*. *Microb Biotechnol.* 2014;7(5):456–66.
26. Gao Z, et al. Butyrate Improves Insulin Sensitivity and Increases Energy Expenditure in Mice. *Diabetes.* 2009;58(7):1509–17.
27. Qin J, et al. A metagenome-wide association study of gut microbiota in type 2 diabetes. *Nature.* 2012;490(7418):55–60.
28. Karlsson FH, et al. Gut metagenome in European women with normal, impaired and diabetic glucose control. *Nature.* 2013;498(7452):99–103.
29. Le Roy T, et al. *Dysosmobacter welbionis* is a newly isolated human commensal bacterium preventing diet-induced obesity and metabolic disorders in mice. *Gut.* 2022;71:534–43.
30. Smith U, Kahn BB. Adipose tissue regulates insulin sensitivity: role of adipogenesis, de novo lipogenesis and novel lipids. *J Intern Med.* 2016;280(5):465–75.
31. Brady MJ. IRS2 takes center stage in the development of type 2 diabetes. *J Clin Invest.* 2004;114(7):886–8.
32. Morrison DJ, Preston T. Formation of short chain fatty acids by the gut microbiota and their impact on human metabolism. *Gut microbes.* 2016;7(3):189–200.
33. den Besten G, et al. Gut-derived short-chain fatty acids are vividly assimilated into host carbohydrates and lipids. *Am J Physiol Gastrointest Liver Physiol.* 2013;305(12):G900–10.
34. den Besten G, et al. Short-chain fatty acids protect against high-fat diet-induced obesity via a PPAR $\gamma$ -dependent switch from lipogenesis to fat oxidation. *Diabetes.* 2015;64(7):2398–408.
35. Lymperopoulos A, Suster MS, Borges JJ. Short-chain fatty acid receptors and cardiovascular function. *Int J Mol Sci.* 2022;23(6).
36. Berkovitch F, et al. A locking mechanism preventing radical damage in the absence of substrate, as revealed by the x-ray structure of lysine 5,6-aminomutase. *Proc Natl Acad Sci.* 2004;101(45):15870–5.
37. Semba RD, et al. Plasma carboxymethyl-lysine, an advanced glycation end product, and all-cause and cardiovascular disease mortality in older community-dwelling adults. *J Am Geriatr Soc.* 2009;57(10):1874–80.
38. Cai W, et al. Oral advanced glycation endproducts (AGEs) promote insulin resistance and diabetes by depleting the antioxidant defenses AGE receptor-1 and sirtuin 1. *Proc Natl Acad Sci.* 2012;109(39):15888–93.
39. Basta G, Schmidt AM, De Caterina R. Advanced glycation end products and vascular inflammation: implications for accelerated atherosclerosis in diabetes. *Cardiovasc Res.* 2004;63(4):582–92.
40. Luevano-Contreras C, Chapman-Novakofski K. Dietary advanced glycation end products and aging. *Nutrients.* 2010;2(12):1247–65.
41. Bui TPN, et al. *Intestinimonas*-like bacteria are important butyrate producers that utilize Ne-fructosyllysine and lysine in formula-fed infants and adults. *J Funct Foods.* 2020;70:103974.
42. Oh TJ, et al. Butyrate attenuated fat gain through gut microbiota modulation in db/db mice following dapagliflozin treatment. *Sci Rep.* 2019;9(1):20300.
43. Brown AJ, et al. The Orphan G protein-coupled receptors GPR41 and GPR43 are activated by propionate and other short chain carboxylic acids. *J Biol Chem.* 2003;278(13):11312–9.
44. Le Poul E, et al. Functional characterization of human receptors for short chain fatty acids and their role in polymorphonuclear cell activation. *J Biol Chem.* 2003;278(28):25481–9.
45. Samuel BS, et al. Effects of the gut microbiota on host adiposity are modulated by the short-chain fatty-acid binding G protein-coupled receptor, Gpr41. *Proc Natl Acad Sci U S A.* 2008;105(43):16767–72.
46. Vinolo MA, et al. Suppressive effect of short-chain fatty acids on production of proinflammatory mediators by neutrophils. *J Nutr Biochem.* 2011;22(9):849–55.
47. Usami M, et al. Butyrate and trichostatin A attenuate nuclear factor  $\kappa$ B activation and tumor necrosis factor  $\alpha$  secretion and increase prostaglandin E2 secretion in human peripheral blood mononuclear cells. *Nutr Res.* 2008;28(5):321–8.
48. Inan MS, et al. The luminal short-chain fatty acid butyrate modulates NF- $\kappa$ B activity in a human colonic epithelial cell line. *Gastroenterology.* 2000;118(4):724–34.
49. Bian Z, et al. Sodium Butyrate Inhibits Oxidative Stress and NF- $\kappa$ B/NLRP3 Activation in Dextran Sulfate Sodium Salt-Induced Colitis in Mice with Involvement of the Nrf2 Signaling Pathway and Mitophagy. *Dig Dis Sci.* 2023;68(7):2981–96.
50. Pedersen SS, et al. Butyrate inhibits IL-1 $\beta$ -induced inflammatory gene expression by suppression of NF- $\kappa$ B activity in pancreatic beta cells. *J Biol Chem.* 2022;298(9): 102312.
51. Wang X, et al. Sodium butyrate alleviates adipocyte inflammation by inhibiting NLRP3 pathway. *Sci Rep.* 2015;5(1):12676.
52. Wu H, Ballantyne CM. Metabolic inflammation and insulin resistance in obesity. *Circ Res.* 2020;126(11):1549–64.
53. De Nardo D, Latz E. NLRP3 inflammasomes link inflammation and metabolic disease. *Trends Immunol.* 2011;32(8):373–9.
54. Modica S, et al. Expression and localisation of insulin receptor substrate 2 in normal intestine and colorectal tumours. Regulation by intestine-specific transcription factor CDX2. *Gut.* 2009;58(9):1250–9.
55. Liang H, Ward WF. PGC-1 $\alpha$ : a key regulator of energy metabolism. *Adv Physiol Educ.* 2006;30(4):145–51.
56. Hao F, et al. Butyrate enhances CPT1A activity to promote fatty acid oxidation and iTreg differentiation. *Proc Natl Acad Sci.* 2021;118(22):e2014681118.
57. Hong J, et al. Butyrate alleviates high fat diet-induced obesity through activation of adiponectin-mediated pathway and stimulation of mitochondrial function in the skeletal muscle of mice. *Oncotarget.* 2016;7(35):56071–82.
58. Aguilar EC, et al. Sodium butyrate modulates adipocyte expansion, adipogenesis, and insulin receptor signaling by upregulation of PPAR- $\gamma$  in obese Apo E knockout mice. *Nutrition.* 2018;47:75–82.
59. Zuriaga MA, et al. Humans and mice display opposing patterns of “browning” gene expression in visceral and subcutaneous white adipose tissue depots. *Front Cardiovasc Med.* 2017;4:7.
60. Maassen K, et al. Habitual intake of dietary dicarbonyls is associated with greater insulin sensitivity and lower prevalence of type 2 diabetes: the Maastricht study. *Am J Clin Nutr.* 2023;118(1):151–61.
61. Wu Y, et al. The metabolism and transformation of casein-bound lactulosyllysine in vivo: Promoting dicarbonyl stress and the formation of advanced glycation end products accompanied by systemic inflammation. *Food Chem.* 2024;444:138681.
62. Singh VP, et al. Advanced glycation end products and diabetic complications. *Korean J Physiol Pharmacol.* 2014;18(1):1–14.
63. Yamagishi S, et al. Role of advanced glycation end products (AGEs) and oxidative stress in vascular complications in diabetes. *Biochim Biophys Acta.* 2012;1820(5):663–71.
64. Pruesse E, Peplies J, Glöckner FO. SINA: accurate high-throughput multiple sequence alignment of ribosomal RNA genes. *Bioinformatics.* 2012;28(14):1823–9.
65. Ludwig W, et al. ARB: a software environment for sequence data. *Nucleic Acids Res.* 2004;32(4):1363–71.
66. Stams AJM, et al. Growth of syntrophic propionate-oxidizing bacteria with fumarate in the absence of methanogenic bacteria. *Appl Environ Microbiol.* 1993;59(4):1114–9.
67. Liao Y-C, et al. MyPro: A seamless pipeline for automated prokaryotic genome assembly and annotation. *J Microbiol Methods.* 2015;113:72–4.
68. Andrews S. FastQC A quality control tool for high throughput sequence data. Available from: citeulike-article-id:1158382772.
69. Zerbino DR, Birney E. Velvet: Algorithms for de novo short read assembly using de Bruijn graphs. *Genome Res.* 2008;18(5):821–9.

70. Hernandez D, et al. De novo bacterial genome sequencing: Millions of very short reads assembled on a desktop computer. *Genome Res.* 2008;18(5):802–9.
71. Luo R, et al. SOAPdenovo2: an empirically improved memory-efficient short-read de novo assembler. *GigaScience.* 2012;1(1):1–6.
72. Bankevich A, et al. SPAdes: a new genome assembly algorithm and its applications to single-cell sequencing. *J Comput Biol.* 2012;19(5):455–77.
73. Husemann P, Stoye J. r2cat: synteny plots and comparative assembly. *Bioinformatics.* 2010;26(4):570–1.
74. Aziz R, et al. The RAST server: Rapid annotations using subsystems technology. *BMC Genomics.* 2008;9(1):75.
75. Finn RD, et al. Pfam: the protein families database. *Nucleic Acids Res.* 2014;42(D1):D222–30.
76. Hunter S, et al. InterPro in 2011: new developments in the family and domain prediction database. *Nucleic Acids Res.* 2012;40(10):4725.
77. Russell A, et al. Reduced housing density improves statistical power of murine gut microbiota studies. *Cell Rep.* 2022;39(6): 110783.
78. Mazzoli A, et al. Modulation of the Nuclear factor erythroid 2-related factor 2 (Nrf2) pathway by the probiotic *Limosilactobacillus reuteri* DSM 17938 prevents diet-induced rat brain dysfunction. *J Funct Foods.* 2024;116:106162.
79. Rampanelli E, Romp N, Troise AD, Ananthasabesan J, Wu H, Gül IS, et al. Gut bacterium *Intestinimonas butyriciproducens* improves host metabolic health: evidence from cohort and animal intervention studies. 2024. Preprint. <https://doi.org/10.21203/rs.3.rs-4364001/v1>

## Publisher's Note

Springer Nature remains neutral with regard to jurisdictional claims in published maps and institutional affiliations.